Lava flow hazard modelling during the 2021 Fagradalsfjall eruption, Iceland: Applications of MrLavaLoba

Gro B. M. Pedersen[1], Melissa A. Pfeffer[2], Sara Barsotti[2], Simone Tarquini[3], Mattia de´ Michieli Vitturi[3,4], Bergrún A. Óladóttir[1,2], Ragnar Heiðar Þrastarson[2]

[1]Nordic Volcanological Center, Institute of Earth Sciences, University of Iceland, Reykjavík, 102, Iceland
[2]Icelandic Meteorological Office, Reykjavík, 105, Iceland
[3]Istituto Nazionale di Geofisica e Vulcanologia, Pisa, 56127, Italy
[4]Department of Geology, University at Buffalo, Buffalo, New York 14260, USA

Correspondence to: Gro B. M. Pedersen (gro@hi.is)+-

Abstract

~~On March 19, 2021, the first eruption on the Reykjanes Peninsula in ca. 800 years took place in~~The 6-month long effusive eruption at Fagradalsfjall volcano in 2021 ~~, in the backyard of the capital Reykjavík. This 6-month long effusive eruption~~ is the most visited eruption in Iceland to date (June, 2023) and it needed intense lava flow hazard assessment. ~~It became a case study for hazard assessment for future eruptions on the Peninsula, which have the potential to issue lava into inhabited areas or inundate essential infrastructure.~~

In this study we document~~ed~~ how lava flow modelling strategies were implemented using the stochastic ~~code~~ model MrLavaLoba, to evaluate hazards during this effusive event. Overall, the purposes were three-fold: (a) Pre-eruption simulations to investigate potential lava inundation of critical infrastructure, (b) Syn-eruptive simulations for short-term (two weeks-timeframe) lava flow hazard assessment and (c) Syn-eruptive simulations for long-term (months to years) hazard assessments. Additionally, strategies for lava barrier testing were developed and syn-eruptive topographic models were incorporated into simulations in near-real time. The model provided promising results that were shared regularly on stakeholder meetings with the monitoring personnel, scientists and civil protection representatives helping to identify potential short-term and long-term lava hazards. This included evaluation of the timing of barrier overflow and the filling and spilling of lavas from one valley to another.

During the crisis the ~~co~~MrLavaLoba model~~de~~ was updated to increase functionalities such as considering multiple active vents. Post-eruption, the model~~code~~ was optimized substantially decreasing the computational time required for the simulations, speeding up the delivery of final products.

1 Introduction

On March 19, 2021, the first eruption on the Reykjanes Peninsula in ca. 800 years started at Mt. Fagradalsfjall, a mountainous area cut by nested enclosed valleys (Fig. 1). Being located in the backyard of the capital Reykjavík and the international airport, ~~this eruption was the most visited eruption in Iceland to date. T~~thousands of people visited the eruption each day, which therefore needed intense monitoring and thorough hazard assessment (Barsotti et al., 2023). The 2021 Fagradalsfjall eruption did not impact any critical infrastructure. However, it became a case study for the monitoring and hazard assessment for future effusive eruptions since several volcanic systems on the Reykjanes peninsula have the potential to issue lava into inhabited areas or inundate critical infrastructure.

To address the varied lava flow hazards during the pre-eruptive unrest phase and during the eruption ~~In this study we document how~~we implemented ~~various~~ different lava flow modelling strategies using the stochastic ~~code~~ model MrLavaLoba (de' Michieli Vitturi and Tarquini, 2018) ~~were implemented during the pre-eruptive unrest phase and during the eruption~~. The ~~code~~model proved to be a useful and a flexible tool to evaluate pre-eruption as well as syn-eruptive short-term and long-term hazards during the 6-month long effusive event. Different approaches as well as new developments of the code were used to account for the changes in the eruptive behavior, and to resolve challenges provided by the complex topographic terrain, where infilling and overflowing of nested valleys created time-evolving hazards for visitors. Additionally, strategies for lava barrier testing were developed and near-real time syn-eruptive topographic models were incorporated as the eruption progressed. We describe in detail the model performance throughout the eruption and at the end we address caveats that should be considered when applying the ~~code~~model and make suggestions for future improvements.

21.1 Geological setting and eruptive history

Reykjanes Peninsula is an oblique spreading zone, characterized by eruptive fissures, open fissures and N-S striking strike-slip faults that are associated with the Mid-Atlantic plate boundary (e.g., Klein et al., 1977; Gee, 1998; Clifton and Kattenhorn, 2006; Einarsson et al., 2020, Sæmundsson et al., 2020). The eruptive centers have been divided into 4 – 6 volcanic systems (Fig. 1c), based on high-temperature geothermal areas, magnetic anomalies, eruptive centers, and geochemistry and are from East to West named: Hengill, Brennisteinsfjöll, Krýsuvík, Fagradalsfjall, Svartsengi and Reykjanes (e.g., Jakobsson et al., 1978; Einarsson and Sæmundsson, 1987; Einarsson et al., 2020, Sæmundsson et al., 2020).

Volcanic activity on the Reykjanes Peninsula has been episodic, with several eruptions occurring in multiple volcanic systems over several hundred years followed by ~800–1000 years of quiescence. During the eruptive cycles of the last four thousand years Reykjanes, Svartsengi, Krýsuvík, Brennisteinsfjöll and Hengill volcanic systems have erupted (Fig. 1c),

while the Fagradalsfjall volcanic system remained inactive (Sæmundsson et al., 2020). The most recent eruptive period of the Reykjanes Peninsula ended in 1240 CE (Sæmundsson et al., 2020). Basaltic subaerial volcanic activity has dominated the Reykjanes Peninsula since the termination of the last glaciation, estimated at around 12,000 – 15,000 years ago (e.g., Jakobsson et al., 1978; Sæmundsson et al., 2010). The axial centers of the volcanic systems are dominated by eruption fissures, while shield volcanos lie on the periphery of each swarm (Jakobsson et al., 1978). The fissure eruptions were presumably short-lived, high effusion rate eruptions, while the shields are believed to be long-lived monogenetic eruptions that dominated the early postglacial times (Rossi, 1996, Jakobsson et al., 1978). During interglacial periods volcanic eruptions formed widespread glaciovolcanic edifices on the peninsula ranging from small mounds, tindars, flat-topped tuyas to multiple, polygenetic complexes of intergrown tindars and tuyas (Jones, 1969, Sæmundsson et al., 2010; Pedersen and Grosse, 2014). Mt. Fagradalsfjall lies in a complex of intergrown tuyas, tindars and mounds of different ages creating a complex of mountains ranging from 100-350 m elevation cut by nested enclosed valleys ranging from 50–215 m elevation. Around this glaciovolcanic complex there are postglacial lava fields gently dipping away from the complex in all directions (Sæmundsson et al., 2010).

~~2.1~~1.2 Fagradalsfjall unrest and eruption

In the following section the Fagradalsfjall 2021 unrest and eruption phases (Figure 2, column 1) are described with a focus on those characteristics of the eruption that affected the lava flow simulations performed at each stage (Figure 2, column 2). Prior to the eruption, volcano-seismic unrest was detected at multiple volcanic systems (Svartsengi, Reykjanes and Krýsuvík) along the Reykjanes Peninsula. Intense seismicity started in December 2019 and ground deformation revealing episodes of inflation and deflation started in January 2020 (Cubuk-Sabuncu et al. 2021, Floventz et al., 2022, Sigmundsson et al., 2022, Greenfield et al., 2022 Barsotti et al., 2023). On February 24, 2021, an intense earthquake swarm began with a M_w 5.64 located 2-4 km NE of Fagradalsfjall marking the start of a dike intrusion. The location of the seismicity was both associated with the dike intrusion and the neighboring faults which were activated by induced stress changes in the crust (Sigmundsson et al, 2022). The dike continued to lengthen to approximately 9 km during the next 23 days before it erupted east of Fagradalsfjall (Sigmundsson et al., 2022).

The eruption began on March 19 between 20:30 to 20:50 UTC in the Geldingadalir valley when a 180 m long fissure opened (Pedersen et al.,2022a, Barsotti et al., 2023). The fissure quickly concentrated into two neighboring vents (Eibl et al., 2023). The lava started infilling the valley with a time-average discharge rate (TADR) ranging from 1 to 8 m^3/s (Pedersen et al., 2022a). By April 5 a new phase of eruptive activity started as two new fissures opened 800 m northeast of the first fissure. Further fissures opened at midnight on April 7, on April 10 and on April 13. Each fissure concentrated into 1–2 circular vents, which over the following 10 days became inactive, except for the southern vent that developed from the April 13 fissures (Barsotti et al., 2023). By April 27 only one vent was active and remained active throughout the rest of the eruption (Barsotti et al., 2023). During this vent migration phase the TADR ranged from 5 to 8 m^3/s (Pedersen et al., 2022a) and the

lava started to flow into the valleys of Meradalir (April 5) and Syðri-Meradalur (April 14). From April 27 to June 28 the TADR increased from 9 m^3/s to a maximum of 13 m^3/s and with this increased effusion rate the lava migrated to its maximum extent 3.3 km from the active vent. The lava was transported in systems of connected channels, lava ponds and tubes (Pedersen et al., in 2022a). The lava "filled and spilled" to Nátthagi valley through Syðri-Meradalir (May 22) and through southern Geldingadalir (June 13). From June 28 to September 2 the lava effusion from the vent changed from being continuous to episodic (ca. 12–24 hours of lava emplacement) followed by inactive periods of similar length (Barsotti et al., 2023). Despite this change, the TADR in this phase was similar to the previous phase ranging from 9 to 11 m^3/s (Pedersen et al., 2022a). The episodic activity disrupted the dominant lava transport system, causing large overflows in the vent region where an additional 50 m of lava piled up increasing the total maximum lava thickness to 124 m (Pedersen et al., 2022a). In the last days of the eruption, September 2 -18, a 9-day-long pause (September 2–11) was followed by a week-long period (September 11-18) of activity (Pedersen et al., 2022a, Barsotti et al., 2023). Most of the lava emplacement was in Geldingadalir, where a 10–15 m thick lava pond was established north-northwest of the active crater between September 11 to 15. The pond partly drained southward through an upwelling zone and into Nátthagi (September 15–18). The measured TADR was 12 m^3/s for September 9–17 and the final bulk volume of the lava flow-field increased to 150.8×10^6 m^3 covering an area of 4.85 km^2 (Pedersen et al., 2022a).

1.~~1~~3. Lava flow simulations

Numerical ~~lava flow modelling codes~~models for the simulation of the emplacement of lava flows ~~emplacement~~ are widely used for hazard and risk assessments purposes before and during eruptions~~. Existing lava flow models~~, and they are often divided into deterministic and stochastic (or probabilistic) ~~codes~~models. The so-called ~~D~~deterministic ~~codes~~ models are intended to mimic the behavior of the natural systems by modeling physical processes based on a set of conservation equations parameters including parameters such as lava discharge rate, lava temperature and heat transfer (e.g., Dietterich et al., 2017, FLOWGO: Harris and Rowland, 2001, PyFLOWGO: Chevrel et al., 2018, MAGFLOW: Cappello et al., 2016a). The s~~S~~tochastic ~~codes~~models ~~capture~~ are based on the evidence that lava is a gravitational flow which tends to follow the steepest path of descent downhill (Favalli et al., 2012), but it can deviate from it in an ~~chaotic~~ unpredictable way (e.g., DOWNFLOW: Favalli et al., 2005, Tarquini and Favalli, 2013, Q-LAVHA: Mossoux et al., 2016). Recent developments of stochastic ~~codes~~ models have included erupted volume as an input parameter allowing the lava field thickness to be one of the model ~~result~~ output (Glaze and Baloga, 2013, MrLavaLoba: de' Michieli Vitturi and Tarquini 2018). The deterministic ~~codes~~ models and some of the stochastic ones attempt to replicate the patterns of channelized lava flows (e.g., Mossoux et al., 2016, Dietrich et al., 2017, Chevrel et al., 2018), while a few stochastic ~~codes~~ models additionally replicate tube-fed flows (Favalli et al., 2005, de' Michieli Vitturi and Tarquini, 2018).

Starting with the pioneering work at Mt. Etna during the 1991-93 eruption (Barberi and Villari, 1994), numerical modeling of lava flows has increasingly been used to mitigate potential destruction caused by active lava flows. This

approach has been refined over the years in both theoretical and practical aspects (e.g., Wright et al., 2008, Cappello et al., 2016a, Harris et al., 2019) including using an operational tool which combines satellite-derived discharge rate estimates and the MAGFLOW numerical code (Vicari et al. 2011, Ganci et al. 2012).

Paths of steepest descent ~~has~~ have been used since 2007 by the Hawaiian Volcano Observatory (HVO) to assess likely lava flow routes during effusive crises (Kauahikaua, 2007). During the 2018 eruption in the Puna district (Neal et al., 2019), the HVO produced preliminary lava flow path forecasts using the DOWNFLOW code (Favalli et al. 2005) to inform about probable future lava flow directions.

At Piton de la Fournaise (La Reunion, France), the local Observatoire Volcanologique du Piton de la Fournaise (OVPF) tackles the hazard related to the frequent effusive eruptions by combining the processing of satellite data with numerical lava flow modeling (Harris et al. 2017, 2019, Peltier et al., 2022). The OVPF has promoted an effective collaboration between scientists affiliated to a multinational array of institutes and is able to issue hazard maps based on DOWNFLOW (Favalli et al., 2005, Chevrel et al., 2021) and PyFLOWGO (Chevrel et al., 2018) within a few hours after the onset of an effusive eruption (Peltier et al., 2020).

In other recent effusive crisis such as the 2014-2015 Fogo eruption, Cape Verde lava flow hazards assessment was performed using both DOWNFLOW (Richter et al., 2016) and MAGFLOW (Cappello et al., 2016b) codes, while the 2021 La Palma eruption used VORIS code (Felpeto et al., 2007; Carracedo et al., 2022; Marti et al., 2022).

1.~~2~~ ~~4~~ Lava flow hazard modelling in Iceland

The first lava flow simulations during an eruption in Iceland was done during the 2010 Fimmvörðuháls eruption with VORIS, which is ~~an~~ a GIS-based program for volcanic hazard assessment (Felpeto et al., 2007, Thorkelsson et al., 2012). The simulation was made to assess potential eruption scenarios with a given eruption location and runout length as input parameters. Prior to the onset of the 2014-2015 Holuhraun eruption, both VORIS ran as part of the VOLCANBOX package (https://volcanbox.wordpress.com/) within the VeTools project (http://www.evevolcanoearlywarning.eu/vetools-objectives/), and the ~~early~~ initial versions of ~~a new Python based stochastic model~~the, MrLavaLoba model ~~started being run (de' Michieli Vitturi and Tarquini, 2018). During the unrest phase before the Holuhraun eruption, both VORIS and MrLavaLoba were run regularly and compared to each other. MrLavaLoba continued to be developed and improved throughout the eruption (Tarquini et al., 2019). After this eruption, both VORIS and MrLavaLoba were used for volcanic hazard assessment projects in Iceland (Andrésdóttir, 2016, 2018; Pfeffer et al., 2020). Since 2015 the Icelandic Meteorological office, the Volcano Observatory in Iceland, has performed lava hazard assessments using the stochastic model MrLavaLoba. Both because of its fast computational time compared to more complex "deterministic" models that that have greater computational requirements, but also because its abilities to account for lava flow volume and the syn-eruptive modification of the topography compared to other stochastic ~~codes~~models.

Formatted: Font: (Default) Times New Roman, 12 pt

Formatted: Line spacing: single

2 Geological setting and eruptive history

Reykjanes Peninsula is an oblique spreading zone, characterized by eruptive fissures, open fissures and N-S striking strike-slip faults that are associated with the Mid-Atlantic plate boundary (e.g., Klein et al., 1977; Gee, 1998; Clifton and Kattenhorn, 2006; Einarsson et al., 2020, Sæmundsson et al., 2020). The eruptive centers have been divided into 4—6 volcanic systems (Fig. 1c), based on high-temperature geothermal areas, magnetic anomalies, eruptive centers, and geochemistry and are from East to West named: Hengill, Brennisteinsfjöll, Krýsuvík, Fagradalsfjall, Svartsengi and Reykjanes (e.g., Jakobsson et al., 1978; Einarsson and Sæmundsson, 1987; Einarsson et al., 2020, Sæmundsson et al., 2020).

Volcanic activity on the Reykjanes Peninsula has been episodic, with several eruptions occurring in multiple volcanic systems over several hundred years followed by ~800–1000 years of quiescence. During the eruptive cycles of the last four thousand years Reykjanes, Svartsengi, Krýsuvík, Brennisteinsfjöll and Hengill volcanic systems have erupted (Fig. 1c), while the Fagradalsfjall volcanic system remained inactive (Sæmundsson et al., 2020). The most recent eruptive period of the Reykjanes Peninsula ended in 1240 CE (Sæmundsson et al., 2020). Basaltic subaerial volcanic activity has dominated the Reykjanes Peninsula since the termination of the last glaciation, estimated at around 12,000 – 15,000 years ago (e.g., Jakobsson et al., 1978; Sæmundsson et al., 2010). The axial centers of the volcanic systems are dominated by eruption fissures, while shield volcanos lie on the periphery of each swarm (Jakobsson et al., 1978). The fissure eruptions were presumably short-lived, high effusion rate eruptions, while the shields are believed to be long-lived monogenetic eruptions that dominated the early postglacial times (Rossi, 1996, Jakobsson et al., 1978). During interglacial periods volcanic eruptions formed widespread glaciovolcanic edifices on the peninsula ranging from small mounds, tindars, flat-topped tuyas to multiple, polygenetic complexes of intergrown tindars and tuyas (Jones, 1969, Sæmundsson et al., 2010; Pedersen and Grosse, 2014). Mt. Fagradalsfjall lies in a complex of intergrown tuyas, tindars and mounds of different ages creating a complex of mountains ranging from 100-350 m elevation cut by nested enclosed valleys ranging from 50–215 m elevation. Around this glaciovolcanic complex there are postglacial lava fields gently dipping away from the complex in all directions (Sæmundsson et al., 2010).

2.1 Fagradalsfjall unrest and eruption

In the following section Fagradalsfjall 2021 unrest and eruption phases (Figure 2, column 1) are described with a focus on those characteristics of the eruption that affected the lava flow simulations performed at each stage (Figure 2, column 2).

Prior to the eruption, volcano-seismic unrest was detected at multiple volcanic systems (Svartsengi, Reykjanes and Krýsuvík) along the Reykjanes Peninsula. Intense seismicity started in December 2019 and ground deformation revealing episodes of inflation and deflation started in January 2020 (Cubuk-Sabuncu et al. 2021, Floventz et al., 2022, Sigmundsson et al., 2022, Greenfield et al., 2022 Barsotti et al., 2023). On February 24, 2021, an intense earthquake swarm began with a M_w 5.64 located 2–4 km NE of Fagradalsfjall marking the start of a dike intrusion. The location of the seismicity was both associated with the dike intrusion and the neighboring faults which were activated by induced stress changes in the crust (Sigmundsson et al, 2022). The dike continued to lengthen to approximately 9 km during the next 23 days before it erupted east of Fagradalsfjall (Sigmundsson et al., 2022).

The eruption began on March 19 between 20:30 to 20:50 UTC in the Geldingadalir valley when a 180 m long fissure opened (Pedersen et al.,2022a, Barsotti et al., 2023). The fissure quickly concentrated into two neighboring vents (Eibl et al., 2023). The lava started infilling the valley with a time-average discharge rate (TADR) ranging from 1 to 8 m^3/s (Pedersen et al., 2022a). By April 5 a new phase of eruptive activity started as two new fissures opened 800 m northeast of the first fissure. Further fissure opened at midnight on April 7, on April 10 and on April 13. Each fissure concentrated into 1–2 circular vents, which over the following 10 days became inactive, except for the southern vent that developed from the April 13 fissures (Barsotti et al., 2023). By April 27 only one vent was active and remained active throughout the rest of the eruption (Barsotti et al., 2023). During this vent migration phase the TADR ranged from 5 to 8 m^3/s (Pedersen et al., 2022a) and the lava started to flow into the valleys of Meradalir (April 5) and Syðri-Meradalur (April 14). From April 27 to June 28 the TADR increased from 9 m^3/s to a maximum of 13 m^3/s and with this increased effusion rate the lava migrated to its maximum extent 3.3 km from the active vent. The lava was transported in systems of connected channels, lava ponds and tubes (Pedersen et al., in 2022a). The lava "filled and spilled" to Nátthagi valley through Syðri-Meradalir (May 22) and through southern Geldingadalir (June 13). From June 28 to September 2 the lava effusion from the vent changed from being continuous to episodic (ca. 12–24 hours of lava emplacement) followed by inactive periods of similar length (Barsotti et al., 2023). Despite this change, the TADR in this phase was similar to the previous phase ranging from 9 to 11 m^3/s (Pedersen et al., 2022a). The episodic activity disrupted the dominant lava transport system, causing large overflows in the vent region where an additional 50 m of lava piled up increasing the total maximum lava thickness to 124 m (Pedersen et al., 2022a). In the last days of the eruption, September 2 -18, a 9-day-long pause (September 2–11) was followed by a week-long period (September 11-18) of activity (Pedersen et al., 2022a, Barsotti et al., 2023). Most of the lava emplacement was in Geldingadalir, where a 10–15 m thick lava pond was established north-northwest of the active crater between September 11 to 15. The pond partly drained southward through an upwelling zone and into Nátthagi (September 15–18). The measured TADR was 12 m^3/s for September 9–17 and the final bulk volume of the lava flow field increased to $150.8 \times 10^6 m^3$ covering an area of 4.85 km^2 (Pedersen et al., 2022a).

~~3 Data and Methods~~

~~2~~3.1 Data

The primary data sources for lava flow simulations were the pre-eruptive and syn-eruptive digital elevation models (DEMs) that constitute the computational domain for the lava flow simulations.

In the pre-eruptive phase the lava flow simulations were initialized by using predefined, hypothetical, longer-term scenarios characterized by different total volumes and fissure lengths. Two main volumetric eruptive scenarios were considered based on data from the eruptive history of Reykjanes Peninsula (Sigurgeirsson and Einarsson, 2016; Einarsson, 2019a,b; Saemundsson, 2019; Sigurgeirsson and Einarsson, 2019; Óladóttir, 2022); comprising a small and a medium-sized scenario characterized by volumes <0.1 km^3 and 0.1-0.5 km^3, respectively. Two lava flow fields: Illahraun (0.02 km^3) and Arnarseturhraun (0.3 km^3) served as a template for these scenarios (Sæmundsson et al., 2010). Two fissure lengths were chosen based on Jónsson (1978)´s geological data for the Reykjanes Peninsula; namely short fissures (2 km) and long fissures (10 km). Input data for the syn-eruptive phase relied on observations of extruded volume and vent geometry (Pedersen et al., 2022a, 2022b) and were used for initializing simulations to produce the short-term and long-term hazard assessment.

~~3~~2.~~1.~~1 Pre-eruption DEM

We used the 2 m-cell size IslandsDEMv0 (atlas.lmi.is/dem) as the pre-eruption DEM, a seamless mosaic of the ArcticDEM (Porter et al., 2018), with an improved positional accuracy and reduced amount of data outliers. Based on comparisons with lidar surveys carried out in the vicinity of the Icelandic glaciers (Jóhannesson et al., 2013), the elevation accuracy of the pre-eruption IslandsDEMv0 is better than 0.5 m (https://gatt.lmi.is/geonetwork/srv/eng/catalog.search#/metadata/e6712430-a63c-4ae5-9158-c89d16da6361). The cell size and number of cells of the computational domain (i.e., the DEM in grid format representing the local topography) has a strong impact on the performance of the MrLavaLoba code (Tarquini et al., 2019),- as the number of grid cells increases, the simulation time increases. The IslandsDEMv0 was therefore down sampled depending on the expected spatial extent of simulated scenarios. Long-term scenarios (volume > 0.02 km^3) were simulated on 10 m cell size grids~~.~~, while smaller short-term scenarios (volume < 0.02 km^3) were simulated on 5 m cell size grids. In a few simulations of lava flows close to barriers or within a narrow valley setting, the full resolution 2 m cell size of the IslandsDEMv0 was used as computational domain. We note that the use of a 5 or 10 m cell size DEM is customary in lava flow modeling (Flynn et al. 2023) and we only used a 2 m cell size DEM when a higher detail was necessary.

~~3~~2.~~1.~~2 Syn-eruption photogrammetric surveys

Throughout the eruption, photogrammetric surveys were acquired as a part of the near real-time monitoring of the Fagradalsfjall 2021 eruption. These surveys consisted mainly of aerial photographs and Pléiades stereoimages and by

September 30, 2021, 32 syn-eruptive surveys had been carried out. The acquisition and processing of these surveys are described in detail in Pedersen et al. (2022a) ~~mainly following the semi-automated workflow of Belart et al. (2019) using the software MicMac (Pierrot-Deseilligny et al., 2011, Rupnik et al., 2017), as well as Agisoft Metashape (version 1.7.3) and Pix4D mapper (version 4.6.4).~~. Each of the surveys were co-registered to the pre-eruption DEM, i.e., the IslandsDEMv0, using the DEM co-registration method of the Nuth and Kääb (2011).

Each survey yielded DEMs (2 m cell size) and orthomosaics (0.3 m cell size) from which the lava flow outline was obtained and this data is available via Pedersen et al. (2022b). By subtracting the DEMs with a pre-eruption DEM and with the DEMs from the previous surveys it was possible to obtain thickness maps (2 m cell size) and estimate bulk eruption volumes and time-averaged discharge rates (TADR). These data products were generally available 3–6 hours after acquisition.

The thickness maps were used in the lava flow simulations for two purposes: (a) as comparison to the results of lava flow simulations and (b) to update the computational domain from pre-eruption to syn-eruptive topography for the short-term simulation after April 27, when the lava field had become very complex to simulate due changes in the vent activity and the expansion of the lava field infilling multiple valleys at variable rates.

3~~.2~~ Methods

~~3.2.1 Software~~

MrLavaLoba is a probabilistic lava flow simulation ~~code~~model that was developed starting in 2014 and first released in 2018 (de' Michieli Vitturi and Tarquini, 2018). It is freely available at the model repository (http://demichie.github.io/MrLavaLoba/) and has previously been applied to the following eruptions: Etna 2001, Kilauea 2014–2016, Holuhraun 2014-15 and for hazard assessment of Heimaey (de' Michieli Vitturi and Tarquini, 2018; Tarquini et al., 2019, Pfeffer et al., 2020). A general introduction to the ~~code~~ model is summarized below. For detailed technical explanation of the code, we refer the reader to de' Michieli Vitturi and Tarquini (2018) as well as the ~~above mentioned~~above-mentioned GitHub repository.

The MrLavaLoba ~~code~~ model requires (a) a computational domain constituted by the pre-emplacement topography and (b) a series of input parameters (including e.g., vent(s) position and geometry, total extruded lava volume, the number of computational flows~~, and~~). The lava emplacement is simulated as elliptical lava ~~,~~"parcels"~~"~~ or "lobes" with a given area and thickness that are deposited step-wise along the flow path constantly modifying the topography. Each new parcel buds from an existing one, so that the simulation progresses by creating chains of a ~~specified~~ given number of ~~"~~parcels". The chains of parcels (making up a flow path) are called computational "flows"~~making up a flow path is called a "flow"~~. The direction of propagation of each parcel with respect to the parent parcel (the parcel where the budding process occurs) ~~the flow~~ is determined by the local direction of the steepest ~~path~~ descent path (~~derived from~~computed on the ~~emplacement~~ topography with the addition of a random perturbation) and of an additional contribution (called "inertial factor") given by ~~"inertial"~~

~~factor which considers~~ the direction of the parent parcel ~~(~~(de' Michieli Vitturi and Tarquini 2018)~~with the addition of a random perturbation~~. Once the direction of propagation is determined, the new parcel is added in its final position. Another stochastic variable, the "lobe exponent", controls the probability distribution among the existing parcels to bud ~~to~~ a new ~~lobe~~ parcel. W~~(w~~hen this parameter is set to 0, the latest parcel emplaced ~~generates~~ buds the next ~~lobe~~parcel and no branching occurs~~)~~. The ~~code~~ model proceeds by iteratively setting new parcels on the topography until their ~~total~~ cumulative volume equals th~~ate~~ lava volume prescribed ~~volume~~ for the simulation. At the end of ~~For~~ each simulation the ~~code~~ model provides a raster map of the final lava thickness, where each cell in the raster constitutes the cumulative thickness of all parcels that covered or inundated that cell. The model also ~~and~~ allows saving masked grids obtained by considering inundated cells fulfilling a specified threshold value. As an example, i~~I~~f this threshold is set to 95% (0.95), the thinnest portion of the final lava deposit (i.e. of the map of the final lava thickness) representing 5% of the total volume is disregarded from the map, and constitute a "masked" map of the final lava deposit. ~~results.~~ This step is relevant ~~important~~ due to the probabilistic nature of the model~~code~~, where the thinnest part of the ~~inundated area~~final lava deposit represents a lower probability ~~for~~ of inundation, which ~~and~~ may change between simulations ~~despite having~~with the same input parameters. The 95% masked grids from different simulations with the same input parameters tend to converge (de' Michieli Vitturi and Tarquini, 2018) and represent an area "more likely" to be inundated. Through iterations of a large number of computational flows, MrLavaLoba handles the probabilistic aspect of lava emplacement (de' Michieli Vitturi and Tarquini, 2018).

Additional topographic~~al~~ layers can easily be included in the model, such as lava thickness maps from syn-eruptive surveys or thickness maps of lava barriers allowing quick modification of the pre-emplacement topography (Fig. 3). Several tuning options are implemented to mimic different lava transport mechanisms (channelized flows, lava ~~tunnels~~ tubes or stochastic budding of lava lobes) accounting for a given propensity to lengthening, widening or thickening of the flow field. Examples of input settings written in a largely commented Python code can be found in the code repository (http://demichie.github.io/MrLavaLoba/). Furthermore, specific input parameters used in the pre-eruptive and syn-eruptive phase of the Fagradalsfjall 2021 unrest are provided in Table 1 (overview of the most important input parameters) and Table A1 (all input parameters).

During the Fagradalsfjall eruption several new features have been implemented to improve MrLavaLoba´s applicability to the dynamic event (See section 4). The first change was to add the possibility to have multiple vents (or multiple fissures) active at the same time with a prescribed supply probability. Second, the ~~code~~ model was modified to enable multiple threshold values for a single simulation, to filter inundated areas as differing levels of likelihood of inundation. Finally, the code was optimized to accelerate runs. This improvement was primarily done by providing a faster method to update the topography as new lava parcels are settled by constraining the computationally "expensive" "update topography" function to a very limited area around the new lava parcel. With respect to the version available at the beginning of the Fagradalsfjall

2021 unrest, the optimized code now is up to 5-10 times faster. Appendix B provides details on the specific code changes and when they were implemented.

~~3.2.2 Implementation~~

A flow chart showing the implementation of input data and input parameters for the simulations, simulation results and evaluation can be found in Fig. 3. The implementation of MrLavaLoba ~~code~~ model depended on the purpose of the simulation and Table 1 provides a general overview of the simulation goals, approaches and most important input parameters, while the full set of input parameters can be found in Table A1.

Since MrLavaLoba is a stochastic ~~code~~model, a single simulation~~it~~ does not describe the temporal evolution of the lava emplacement. However, by performing a series of runs simulating different volumes, it is possible to constrain the lava flow-field evolution by using the relationship V= Q * t, where V is volume, Q is the volume flux and t is the time. In the pre-eruption phase Q is a hypothetical effusion rate, while in the syn-eruption phase Q is derived from the TADR measurement performed at a given time (Pedersen et al., 2022a). We scaled the number of computational flows (n_flows) and lobes per computational flow (min_n_lobes and max_n_lobes) as a function of effusion rate and time. Thus, a higher effusion rate would provide more and longer flows from the vent (so larger n_flow and ~~-~~min_n_lobe). With time the number of lobes would also increase (larger min_n_lobe). In this way, insight ~~to~~into the temporal evolution of the lava field could be addressed. The exact tuning of n_flows and min-n-lobe can be found in Table 1 and Table A1.

4 Results

Different lava simulation strategies were implemented during the pre-eruptive unrest and during the eruption depending on the purpose of the simulation (Table 1). Overall, the purposes were three-fold: (a) pre-eruption simulations to investigate the risk to infrastructure, (b) syn-eruptive simulations to investigate short-term (two weeks) lava hazards and (c) syn-eruptive simulations to investigate long-term (months to years) lava hazards.

4.1 Pre-eruption simulations

The pre-eruption lava flow simulations were initiated after seismic and crustal deformation consistent with a 9 km long dike was detected (Sigmundsson et al., 2022). Because of triggered seismicity along neighboring faults a combination of seismic observations, deformation observations and modeling (Sigmundsson et al., 2022) gave the best indication of potential fissure openings. Based on this information 12 different dike openings of 2-10 km length (See 3.1) were chosen for pre-eruptive lava flow simulations (Fig. 4a). Two different strategies were implemented in this unrest phase: (a) short-term ~~worst-case~~large

effusion rate scenarios addressing areas likely to be inundated within a few hours from eruption start (relevant to emergency response planning) and (b) longer-term scenarios to provide insight to areas likely to be inundated within weeks to months (relevant for identification of infrastructure at risk) (Table 1, Fig. 2).

4.1.1 Short-term ~~worst-case~~large effusion rate scenario

The ~~worst-case scenario~~large effusion rate scenario was defined as fissures with an assumed effusion rate of 300 m^3/s, which is considered high effusion rates on Reykjanes Peninsula. We assigned ~~where~~ the number of flows, n_flows = 300 and min_n_lobes were multiplied with 3.33 * per minute to mimic the lengthening of the flows (Table 1, Table A1). This multiplication factor was estimated to be rather high based on the run-out distance from the vent but was preferred rather than being too conservative. The results of the ~~worst-case~~short-term large effusion rate scenarios for the 12 defined dike openings (see example Fig. 4b) suggested that no inhabited areas were in immediate danger during the first hours, and infrastructure was only in danger the first hours if the dike continued propagating south cross-cutting a nearby highway (Fig. 4a). A caveat with this strategy was that the only way to validate the chosen parameter space was based on run-out distance and thickness of final deposit.

4.1.2 Long (er)-term scenario

During the pre-eruption phase the small and medium eruption scenarios were simulated to evaluate potential endangered infrastructures. The tuning of these scenarios had been done before the volcanic unrest in Fagradalsfjall and is described in section 3.1 and input parameters can be found in Table 1 and A1. An example of the moderate scenario is shown in Fig. 4c showing that the only infrastructure in danger was the nearby highway.

4.2 Syn-eruptive simulations: short-term hazard assessments

During the eruption the complexity and demands of the short-term runs increased. Here we describe results from three different approaches applied during the crisis to address the evolution of eruptive activity and the challenges they posed (Fig. 2 and Table 1).

4.2.1 First phase of the eruption: Geldingadalir (March 19-April 5)

The first syn-eruptive runs of MrLavaLoba were started on March 19 around 22:00 UTC (1.5 hours after the eruption started) using preliminary vent coordinates obtained on a helicopter flight. The precise location and length of the fissure was first acquired the following morning when the first aerial images during daylight had been georeferenced. The main purpose of these first runs was to evaluate how the lava would fill the Geldingadalir valleys and when it would spill into Syðri-Meradalur east of Geldingadalir, inundating the hiking path and exposing visitors to lava hazards (Fig. 1, 5, Table 1).

Formatted: Not Highlight

During this phase we used a 180 m fissure erupting with the same rate along its extension, though in reality, the fissure quickly concentrated into two active vents. This was done because mimicking the evolution of the fissure either would have required a major change in the MrLavaLoba code, or a time-consuming, step-wise simulation strategy inconvenient during "emergency-mode" response (Fig 2, column 2 & 3).

The lava simulations were qualitatively evaluated by comparing the thickness maps obtained from photogrammetric surveys with the modelled lava thickness maps. For the first hours of the eruption (<12 hr) the only documentation was from a few oblique photographs. The smallest run (V= 0.018Mm^3) shows northern and southern lobes agreeing with the photographs documenting the extent of the lava at midnight on March 19, ca. 3-4 hr after eruption start (Fig. 5). As the volume increased to 0.2 – 3 Mm^3, the lava simulations overestimated the southern extent of the lava field, whilst underestimating the lava thickness of the northern lobe, which is explained by the closing of the southern part of the fissure. As the volume increased further to 3-7 Mm^3 the modelled results agreed well with the observations suggesting that the lava was so confined by the Geldingadalir valley that the change in vent geometry had little effect on the lava inundation area.

The simulations predicted that at potential exit from Geldingadalir valley into Syðri-Meradalir valley when the volume reached 7 – 10 Mm^3, with slightly different volumes from run to run due to the stochastic nature of the MrLavaLoba code. To provide potential timings of when Geldingadalir would spill into the Syðri-Meradalir valley we used two different effusion rates of 8 m^3/s and 5 m^3/s based on the observed maximum and mean TADR estimates in this phase (Pedersen et al., 2022a). This gave exit times from Geldingadalir of 10-14 days (March 29 -April 2) and 16-24 days (April 4-April 12), respectively. The lava eventually spilled out from Geldingadalir valley on April 14, but by April 5 new vents had opened north of Geldingadalir, with lava draining into Meradalir. By calculating the lava volume within Geldingadalir by April 18 (first photogrammetric survey after lava exited Geldingadalir) we get a volume of 10.8 Mm^3. The 10.8 Mm^3 is in the upper end of the predicted volume of 7 – 10 Mm^3, but taking into account 10.8 Mm^3 is the volume in Geldingadalir four days after the lava spilled into Syðri-Meradalir, we find this in good agreement with the lava simulations.

4.2.2 Second phase: Vent migration (April 5-April 27)

In the second phase the active vents migrated as multiple new fissures opened between April 5-13 and became inactive over the next 10 days, except for one vent (see section 2.1, Fig. 1). This change in eruption activity provided new challenges to the lava flow modelling (Fig. 2). The first challenge was that the topography drastically changed with the new vent openings. While lava was strongly constrained within the Geldingadalir valley in the first phase, after April 5 lava was issued from the plateau NE of Geldingadalir and channelized into narrow gullies before spreading out like a fan within the Meradalir valley. Fissure 2, that opened April 5, had sufficient spacing from Geldingadalir so it could be simulated in a separate run from

Geldingadalir (Fig.6, V< 0.4 Mm^3). However, to capture the channelizing into the narrow valleys it was necessary to increase the resolution of the computational domain DEM (from 5 to 2 m cell size) and change the lobe exponent parameter (from 0.07 to 0.03) increasing the probability of new lobes to be generated by younger lobes (Fig. 2). After this adjustment the new flows were well captured in the simulation (Fig.6, V< 0.4 Mm^3).

After fissure 3 opened on April 7, it was clear that the lava flows from the different vents were influencing each other, and it was therefore necessary to simulate multiple vents that emitted variable percentages of the total lava volume. The MrLavaLoba code was therefore modified to allow this configuration (See section 3.2.1, Fig. 2 and Appendix B). Qualitative estimates on the variable percentages from each vent were based on webcams and direct observations in the field with no direct way of validating these estimates.

As the lava flow field emplacement progressed, it became evident that it was necessary to include the most recent lava thickness maps from the photogrammetric surveys (Pedersen et al., 2022a). By adding the thickness maps on top of the pre-eruption DEM, new simulations were performed on the most updated topography. Examples of two runs with two different vent configurations can be found in figure 6, lowermost panel: one with all vents being active (left) and one performed after the two northernmost vents had shut down (right). These simulations showed how the lava would expand in Geldingadalir and the neighboring valleys: Syðri-Meradalur and Meradalir. However, the expansion in Geldingadalir and the plateau NE were overestimated and the expansion into Meradalir was underestimated. We ascribed this to a problem that we refer to as the "restart problem" (Fig. 2). By restarting the simulation on updated topography, the lava parcels would be initiated from the vents resulting in increased lava deposition close to the vents (explaining the overestimation of Geldingadalir and the plateau NE) and a delay in expansion of the lava field far away from the vents (such as Meradalir) compared to the real flow-field.

4.2.3 Phases three to five: Fill and spill of a highly compound lava flow field (April 27-September 18)

After April 27 the vent activity stabilized at one location (Fig. 1, Vent 5). The mean TADR increased from 6 m^3/s to 11 m^3/s (Pedersen et al., 2022a). The lava flow-field expanded into neighboring valleys such as Nátthagi and further into Meradalir in a "fill and spill" process. There was great interest in simulations that forecasted when and how the lava might overflow from one valley to another e.g., from Geldingadalir into Nátthagi (cross cutting a popular hiking path) or when the lava would exit from the Meradalir valley (inundating a dirt road), or when it would exit Nátthagi (threatening a highway and critical communication cables, as well as approaching the sea). However, due to the restart problem (see 4.2.2) and because the lava discharge into different valleys was highly variable (Pedersen et al., 2022a), it was decided to address these questions related to short-term hazards using worst-case scenario approaches. These scenarios were presented at bi-weekly

stakeholder meetings, where the aim was to identify hazardous areas (upcoming inundation of hiking paths, roads or installed infrastructure) and suggest potential closure of areas to public access (e.g., closing of Nátthagakriki in September 2021).

The short-term worst-case scenarios were defined as a scenario where all lava emitted from the vent would be transported to one of the critical lava margins, e.g., lava margins close to a hiking path or infrastructure that could be inundated by the lava. In these simulations, the most recent TADR estimate (Pedersen et al., 2022a) was used to calculate lava volumes that would be extruded over periods of 3, 7, and 14 days. These volumes were then released at critical lava margins close to valley exits to evaluate if each given volume was sufficient to overflow the valley in the given timeframe. If a 3-day scenario would spill out of the valley, then 6 hr, 12 hr and 24 hr scenarios were additionally modelled~~. The critical locations were selected considering the location of hiking paths and infrastructures~~. In these runs, the input parameter for the "number of flows" (n_flows) was doubled (from 80 to 160, Table 1), both because of the increase of the TADR, and to reduce the uncertainty in the simulation outputs (Fig. 7 in de' Michieli Vitturi and Tarquini, 2018).

An example of how these worst-case scenarios were presented at stakeholder meetings is provided in Fig. 7. To simplify the maps, only the lava inundation areas and not the simulated lava thickness maps were presented in accordance with the stakeholder's interest. The results for the volumes extruded over 3, 7 and 14 days were displayed on one map. The main map (Fig.7a) shows simulations from vent 5 and was considered the most likely scenario, while the four smaller maps show the same volumes released at defined critical locations (Fig.7b-e). As it can be seen by the provided example from September 9, 2021, both the Meradalir, Geldingadalir and Nátthagi valleys had the potential to overflow, if the lava was transported to the critical lava margins. A weakness of this approach was that the locations of critical lava margins were manually selected on the basis of the available knowledge and expert evaluation.

A similar approach was used to test lava barriers that were built or planned to be built during the eruption. An example can be found in Fig. 8, where the overflow of Geldingadalir was simulated with and without barriers based on photogrammetric data from a survey on June 11, 2021. All scenarios show that with 1 Mm^3 volume of lava Geldingadalir would overflow into Nátthagi. In absence of barriers lava would also spill west into Nátthagakriki, but with the proposed barriers it seemed plausible to stall the west-ward migration for small volumes. Once again, these were worst-case scenarios, because (a) they required that the given volume of lava was transported to the critical margin, and (b) the simulations assumed that the transport systems near the barrier promoted the lava piling up near the barrier. However, if an efficient channel or tube developed, most of the lava would be transported into the Nátthagi valley resulting in little lava deposition at the barriers, meaning that the barrier would last longer.

4.3 Long-term runs

Stakeholders (managers of critical infrastructure, municipalities, civil protection authorities) requested long-term scenarios for longer-term planning and we were aiming to provide them in September 2021. The eruption stopped September 18, and these results were therefore only presented at stakeholder meetings. The long-term scenarios were simulated by considering erupted lava volumes ranging between 250 Mm^3 – 5000 Mm^3. Assuming constant mean TADR of 9.5 m^3/s (Pedersen et al., 2022a) across the entire eruption, the simulated long-term scenarios would cover time frames of half a year to decades.

In these large simulations only one vent (vent 5 in Fig. 1) was active throughout the simulation, which had been the case for most of the eruption. Furthermore, each scenario was obtained as a single run (with a single tuning) and not as an iterative process of tuning the model step by step. We tuned the long-term runs against the lava thickness maps obtained in June 2021 having volumes between 53-80 Mm^3 and preferred to overestimate rather than underestimate lava inundation area. Fig. 9 shows that the full extent of the long-term model for 80 Mm^3 (top row, center) fits the real lava deposit very well in both extent and thickness (bottom row, center), except around the NE plateau which is explained by the model only having vent 5 as the active vent. The thickening close to the vent was underestimated and the thickening in Meradalir was overestimated.

The long-term hazard assessment was specifically intended for stakeholders with no experience with lava flow simulation and like the short-term worst-case scenario maps produced in phase 3-5 (See section 4.2.3, Table 1) we choose only to display the lava inundation area, since this was the main interest to stakeholders. The new challenge was how to communicate the uncertainty in our results to non-experts (Pallister et al., 2019). We decided to create maps where lava inundation would be divided into three qualitative categories: “more likely”, “likely” and “less likely” (Fig. 9, left bottom row). We defined the “more likely” category to be the 95% masked grid (See 3.2.1), which filter out the places least likely to be inundated (Fig. 9 top left). The full extent of the lava simulation was decided to be categorized as “likely” (Fig. 9 top center). For the “less-likely” category we wanted to communicate the uncertainty related to the model tuning. We tuned the model when the lava flow field was highly constrained by the surrounding topography. However, in a large eruption the lava would escape the confining valleys and be able to spread more freely over flat-lying areas. To display this uncertainty, it was decided to change the tuning of the “lobe exponent” (from 0.02 to 0.01) which is crucial parameter for the lava flow spreading. A lower lobe exponent promotes lower flow thickness and a longer run out length as revealed in our tuning data set overestimating the inundation area (Fig. 9 top right). We therefore defined this as the “less likely” category.

One example of the long-term hazard maps can be found in Fig.10. The most important message for the authorities from these long-term simulations was that none of the runs reached Grindavík town nor the Svartsengi powerplant, which were the two main areas of concern. We underlined that these long-term runs were quite uncertain, because as the scenario grows in volume so does the uncertainty. Some factors contributing to uncertainty were: (a) tuning being undertaken while the lava

was highly controlled by topography, (b) changes in eruptive activity from continuous (May-June, when tuning were performed) to episodic activity (July-September) and (c) MrLavaLoba does not include vent processes such as cone build-up. The latter was important because the real vent built up faster than predicted in the simulation, meaning that the lava flows could ~~inundated~~inundate Fagradalsfjall faster than predicted in these models.

5 Discussion

5.1 MrLavaLoba code: Advantages and disadvantages

The MrLavaLoba ~~code~~ model is freely available, easy to run, coded in Python, computationally fast and can therefore be used to tackle large volume scenarios (Table 2). Unlike other stochastic ~~codes~~ models it accounts for lava volume ~~and estimates final lava extent~~, it produces lava thickness layers, and it models ongoing topographic changes during the simulation. These characteristics were very important during the Fagradalsfjall 2021 eruption, because assessing the timing of hazards related to the fill and spill of nested valley systems could only be addressed by codes that accounted for lava volume. It was easy to implement topographic changes into the model, including the syn-eruptive differential DEMs of the lava flow thickness and lava barriers, which was key for testing both hypothetical barriers and built lava barriers (Table 2). However, ~~there were~~we also highlight weaknesses~~: to the code:~~ MrLavaLoba model does not provide temporal evolution of the lava field during each run, nor does it directly provide velocity estimates of the lava emplacement (Table 2). Input parameters must be tuned for specific eruptive scenarios and locations. It is possible to mimic different lava emplacement processes (e.g., lava channels or tubes), but this must be tuned as well. Furthermore, the ~~code~~ model does not include vent-processes, which lead to an underestimation of the lava thickness close to the vent for the long-term scenarios. However, to our knowledge, no existing lava simulation code includes vent-processes, so this issue would also have affected any other lava flow simulation ~~code~~models.

5.2 Towards improved modelling

To improve our communication of uncertainty of the lava simulations MrLavaLoba was upgraded in September 2021 to enable multiple masked lava thickness grids (section 3.2.1, appendix B). In the future we can therefore provide maps with uncertainty comprised of the full extent (100 % mask) of the lava flow simulation, the 95% mask and e.g., the 68% mask indicating the likelihood of inundation. In addition, we would like to evaluate of the uncertainty of the input parameters themselves, which can be addressed by using statistical tools such as Dakota (Adams et al., 2021), which specifically designed to perform sensitivity analysis and uncertainty quantification with existing numerical codes (Fig, 3 see bottom row).

In the Fagradalsfjall 2021 eruption the lava flow simulations were evaluated qualitatively (Table 1, Fig. 3), but a quantitative approach would have been preferred. For future eruptions we would like to automate a quantitative comparison between two rasters (e.g., simulation and observation) with respect to the accuracy of the estimated (a) lava inundation area and (b) lava thickness. This can be done by using the Python script *union_diff.py* available in the model repository (http://demichie.github.io/MrLavaLoba/), which permits such comparisons (Fig, 3 see bottom row).

Vent changes (temporal change in vent configuration and geometry, vent build-up and collapse) remained a challenge for the lava simulations during the eruption. This problem was partly solved in April 2021 when the MrLavaLoba code was upgraded to simulate multiple vents (See section 3.2.1, appendix B) and thus the modeler initialized a new lava simulation when the number of active vents changed. Doing step-wise simulations was possible since we could do simulations on updated topography. This strategy has been intended as a route to improve lava flow simulations and reproduce the lava flow-fields more consistently (Harris et al., 2016, Tarquini et al., 2018). However, as we discovered, updating the topographic domain created a new problem, namely the " restart problem" (See 4.2.2): the re-initialized simulation experienced a delay in the lava field expansion. This problem is not unique to MrLavaLoba, but relevant for all lava flow simulation code that intend to do step-wise simulations. Some potential ways forward to solve this could include introducing "spin up"-time that will re-establish activity to the flow field edges, or implement additional sources at active lava margins as we did for the worst-case scenario runs (See 4.2.3).

Finally, a remaining challenge is related to changing the spatial resolution of computational domain in the simulations. Some input parameters need to be re-tuned if the input DEM resolution is changed. Tuning takes time, which is inconvenient during an on-going eruption. As a rule of thumb, the lobe area is 10 x (DEM cell size)^2. If the lobe area changes by a factor G, the number of lobes should change by a factor 1/sqrt(G) for scenarios with a lobe exponent= 0. For other scenarios experimentation with the code and different DEM resolutions could provide us with an automatically applied scaling of these sensitive parameters in case of DEM resolution changes.

5.3 Improved dissemination strategies

During this prolonged volcanic crisis, delivering information on lava flow hazard assessment was a complicated task and identifying good strategies to do it was a learning process. Two main elements were eventually considered when designing map layouts and content: (a) which kind of stakeholders would receive the information and which role did they have during the crisis (e.g., experts, civil defense/responders, decision makers or the public) and (b) which information they needed to receive to fulfill their operations and tasks.

During the eruption regular and frequent meetings were held between monitoring personnel on duty, scientists, ~~Civil~~ civil protection representatives, local police and rangers who were patrolling the area. For the first months they were held daily,

and eventually they held were bi-weekly. Lava flow invasion maps were shown and discussed at these briefings (Barsotti et al. 2023), as well as during dedicated meetings and were occasionally reiterated based on feedback provided by the users.

Thanks to this interaction with the stakeholders, it became clear that the main products for them were the short-term scenarios, short-term worst-case scenarios (Fig.7) and the long-term scenarios (Fig.10). The maps were prepared by following three main criteria: (a) simple maps showing potential lava inundation areas, and not lava thicknesses, (b) showing the uncertainty related to the model results, and (c) including all key- information (e.g., name of lava simulation model, key input parameters, time-frame and main assumptions) to ensure that final product would be self-explaining, even if a figure caption inadvertently was separated from the map. Thus, we were providing multiple map products and customizing them to user needs, which is in accordance with volcano observatory best practices workshops (Pallister et al., 2019, Lowenstern et al., 2022). Distributing maps for the public was complicated and required several iterations and double-checking from experts, to avoid that results triggered many questions and alarmed the community (See e.g., maps made publicly available on the Icelandic Meteorological office's website :https://www.vedur.is/um-vi/frettir/vel-fylgst-med-skjalftahrinunni-vid-keili and https://www.vedur.is/um-vi/frettir/hraunflaedilikon-hafa-sannad-sig-i-eldgosinu-vid-fagradalsfjall).

As described above (section 5.1 and 5.2) including the uncertainty of the lava simulation results, required changes to the ~~simulation code~~model, and in the modelling approach, which, to begin with was requiring extra time. However, it also became clear that when we had efficient ways to include uncertainty in the simulation results, the modeler could (a) avoid time-consuming fine tuning of input parameters, (b) save time in the map production and (c) be much more efficient in communicating the results in a consistent way.

For the next volcanic crisis, the goal is to have pre-formatted map templates for short-term scenarios, short-term worst-case scenarios and the long-term scenarios similar to Fig. 7, 8 and 10. These should be developed collaboratively with hazard and cartography experts to help the lava flow modelers to find a suitable balance between essential information and readability. Secondly, an explanation of the lava hazard modelling approach should be prepared in multiple languages to accompany the maps when communicated to the public. Finally, it would be helpful to discriminate between design of map products delivered to (a) scientific community, (b) stakeholders and (c) the public and potentially set-up some a priori agreements about what type of results should be disseminated to each group and consider appropriate the platform for such information (websites, web map services, social media).

6 Conclusions

After 23 days of volcanic unrest, the eruption at Fagradalsfjall started March 19, 2021 and lasted 6 month. The lava flow hazards varied during this event due to the changes in eruptive activity and due to the complex topographic setting where

lava was infilling a nested valley system. This study address how these varied lava flow hazards were ~~On March 19 to September 18, 2021, the first eruption in ca. 800 years took place on the Reykjanes Peninsula, Iceland. Located in the backyard of the capital Reykjavík and the international airport, this effusive eruption was the most visited eruption in Iceland to date and needed intense monitoring and thorough lava hazard assessment. The eruption harmed no critical infrastructure and became a case study for the monitoring and hazard assessment for future eruptions.~~

~~In this study we documented how~~ evaluated by ~~various~~implementing different ~~-~~lava flow simulation strategies using the stochastic ~~code~~model MrLavaLoba ~~were used to evaluate hazards during the 6-month long effusive event~~. Pre-eruption simulations were performed to investigate exposure of critical infrastructure to lava flow inundation~~Different lava simulation strategies were deployed and their overall, the purposes were three-fold: (a) pre-eruption simulations to investigate exposure of critical infrastructure to lava flow inundation, ~~, while syn-eruptive ~~(b)~~ simulations were addressing short-term (weeks) lava hazards and worst-case scenarios. Finally, ~~and (c)~~ simulations were performed to address long-term (months to years) ~~ing long-term (months to years)~~ lava hazards.

MrLavaLoba provides final lava extent, lava thickness layers and it continually modifies the topography during the simulation. This was very important during the Fagradalsfjall 2021 crisis because the timing of the filling and spilling from one valley to another could not have been addressed by codes not including lava volume. It is very easy to implement topographic changes, e.g., by implementing lava flow thickness maps obtained during the eruption or lava barriers, a key functionality of the code that made it suitable for testing suggested and built lava barriers. As the eruption got more complex, weaknesses of the lava flow simulation came into light. Some input parameters required time-consuming tuning when the spatial resolution of the runs was changed, a" restart problem" related to step-wise simulations with updated topography caused delayed activation of lava flow margins, and challenges relating to time-evolving changes in eruption style.

During the crisis the MrLavaLoba ~~code~~ model was improved to increase functionalities including multiple eruption vents simultaneously and produce multiple lava thickness masks. The former was important during the vent migration phase, while the latter was necessary to communicate uncertainty in model results.
Future scientific improvements could include strategies to automate quantitative evaluations of model results, quantitative uncertainty analysis of input parameters and prepared map templates to efficiently disseminate results.
The lava flow model results were shared regularly with the scientific community, the agencies responsible for the operations in-situ and to the public (through news articles on institutions websites). The numerical code and the established modelling procedures are considered to have been very successful in responding to an eruption that ~~called to~~called tourists and visitors from all over the world.

7 Code and Data availability

MrLavaLoba is code was published in 2018 (d'' Michieli Vitturi and Tarquini, 2018) and is freely available at the model repository (http://demichie.github.io/MrLavaLoba/). Relevant data for this study can be found in Pedersen et al. (2022b), https://doi.org/10.5281/zenodo.6581470. The outputs of MrLavaLoba simulations are available upon request to the corresponding author.

Author contributions

GBMP undertook manuscript preparation, model implementation, strategy development, validation, and formal analysis, and communication with stakeholders. MAP undertook the background research, model implementation for pre-eruption runs, formal analysis, communication with stakeholders and review of manuscript. SB undertook the background research, supervised strategy development and stakeholder contact and review of the manuscript. ST and MdMV developed the code, supervised strategy development and code implementation and reviewed the manuscript. BÓ undertook the background research and reviewed the manuscript and RHÞ contributed to map production and review of the manuscript.

Competing interests

The contact author has declared that neither they nor their co-authors have any competing interests.

Acknowledgements

The authors would like to acknowledge scientists and stakeholders providing feedback on the communication of hazard maps during stakeholder meetings. Furthermore, they would like to thank an anonymous reviewer as well as Freysteinn Sigmundsson who provided an image of the eruption used in figure 5. Finally, we would like to thank our financial support.

Financial support

This research has been supported by the Icelandic Research fund; Grant No. 206755-052 awarded to GBMP.

References

Adams, B.M., Bohnhoff, W.J., Dalbey, K.R., Ebeida, M.S., Eddy, J.P., Eldred, M.S., Hooper, R.W., Hough, P.D., Hu, K.T., Jakeman, J.D., Khalil, M., Maupin, K.A., Monschke, J.A., Ridgway, E.M., Rushdi, A.A., Seidl, D.T., Stephens, J.A., Swiler, L.P., and Winokur, J.G.: Dakota, A Multilevel Parallel Object-Oriented Framework for Design Optimization, Parameter Estimation, Uncertainty Quantification, and Sensitivity Analysis: Version 6.15 User's Manual, Sandia Technical Report SAND2020-12495, November 2021.

Andrésdóttir, Þ. B.: Eldfjallavá á Reykjanesi, Thesis, 2016.

Andrésdóttir, Þ. B.: Volcanic hazard and risk assessment at Reykjanes, vulnerability of infrastructure, Thesis, 2018.
Barberi, F. and Villari, L.: Volcano monitoring and civil protection problems during the 1991–1993 Etna eruption. Acta Vulcanologica, 4, 157-165, 1994.
Barsotti, S., Parks, M. M., Pfeffer, M. A., Óladóttir, B. A., Barnie, T., Titos, M. M., Jónsdóttir, K., Pedersen, G. B. M., Hjartardóttir, Á. R., Stefansdóttir, G., Johannsson, T., Arason, Þ., Gudmundsson, M. T., Oddsson, B., Þrastarson, R. H., Ófeigsson, B. G., Vogfjörd, K., Geirsson, H., Hjörvar, T., von Löwis, S., Petersen, G. N., and Sigurðsson, E. M.: The eruption in Fagradalsfjall (2021, Iceland): how the operational monitoring and the volcanic hazard assessment contributed to its safe access, Nat Hazards, 116, 3063–3092, https://doi.org/10.1007/s11069-022-05798-7, 2023.
~~Belart, J. M. C., Magnússon, E., Berthier, E., Pálsson, F., Aðalgeirsdóttir, G., and Jóhannesson, T.: The geodetic mass balance of Eyjafjallajökull ice cap for 1945–2014: processing guidelines and relation to climate. J. Glaciol. 65, 395–409. Doi: 10.1017/jog.2019.16, 2019.~~
Cappello, A., Ganci, G., Calvari, S., Pérez, N. M., Hernández, P. A., Silva, S. V., Cabral, J., and Del Negro, C.: Lava flow hazard modeling during the 2014–2015 Fogo eruption, Cape Verde. Journal of Geophysical Research: Solid Earth, 121(4), 2290–2303. https://doi.org/10.1002/2015JB012666, 2016a.
Cappello, A., Hérault, A., Bilotta, G., Ganci, G., and Del Negro, C.: MAGFLOW: a physics-based model for the dynamics of lava-flow emplacement, Geological Society, London, Special Publications, 426, 357–373, https://doi.org/10.1144/SP426.16, 2016b.
Carracedo, J. C., Troll, V. R., Day, J. M. D., Geiger, H., Aulinas, M., Soler, V., Deegan, F. M., Perez-Torrado, F. J., Gisbert, G., Gazel, E., Rodriguez-Gonzalez, A., and Albert, H.: The 2021 eruption of the Cumbre Vieja volcanic ridge on La Palma, Canary Islands, Geology Today, 38, 94–107, https://doi.org/10.1111/gto.12388, 2022.
Chevrel, M. O., Favalli, M., Villeneuve, N., Harris, A. J. L., Fornaciai, A., Richter, N., Derrien, A., Boissier, P., Di Muro, A., and Peltier, A.: Lava flow hazard map of Piton de la Fournaise volcano, Natural Hazards and Earth System Sciences, 21, 2355–2377, https://doi.org/10.5194/nhess-21-2355-2021, 2021.
Chevrel, M. O., Labroquère, J., Harris, A. J. L., and Rowland, S. K.: PyFLOWGO: An open-source platform for simulation of channelized lava22hermoso-rheological properties. Computers & Geosciences, 111, 167–180. https://doi.org/10.1016/j.cageo.2017.11.009, 2018.
Clifton, A. E., and Kattenhorn, S. A.: Structural architecture of a highly oblique divergent plate boundary segment. Tectonophysics, 419(1), 27–40. https://doi.org/10.1016/j.tecto.2006.03.016, 2006.
Cubuk-Sabuncu, Y., Jónsdóttir, K., Caudron, C., Lecocq, T., Parks, M. M., Geirsson, H., and Mordret, A.: Temporal Seismic Velocity Changes During the 2020 Rapid Inflation at Mt. Þorbjörn-Svartsengi, Iceland, Using Seismic Ambient Noise, Geophysical Research Letters, 48, e2020GL092265, https://doi.org/10.1029/2020GL092265, 2021.
de' Michieli Vitturi, M., and Tarquini, S.: MrLavaLoba: A new probabilistic model for the simulation of lava flows as a settling process. Journal of Volcanology and Geothermal Research, 349, 323–334. https://doi.org/10.1016/j.jvolgeores.2017.11.016, 2018.
Dietterich, H. R., Lev, E., Chen, J., Richardson, J. A., and Cashman, K. V.: Benchmarking computational fluid dynamics models of lava flow simulation for hazard assessment, forecasting, and risk management. Journal of Applied Volcanology, 6(1), 9. https://doi.org/10.1186/s13617-017-0061-x, 2017.
Eibl, E. P. S., Thordarson, T., Höskuldsson, Á., Gudnason, E. Á., Dietrich, T., Hersir, G. P., and Ágústsdóttir, T.: Evolving shallow conduit revealed by tremor and vent activity observations during episodic lava fountaining of the 2021 Geldingadalir eruption, Iceland, Bull Volcanol, 85, 10, https://doi.org/10.1007/s00445-022-01622-z, 2023.
Einarsson, P., Hjartardóttir, Á. R., Hreinsdóttir, S., and Imsland, P.: The structure of seismogenic strike-slip faults in the eastern part of the Reykjanes Peninsula Oblique Rift, SW Iceland. Journal of Volcanology and Geothermal Research, 391, 106372. https://doi.org/10.1016/j.jvolgeores.2018.04.029, 2020.
Einarsson, P., and Sæmundsson, K.: Earthquake epicenters 1982-1985 and volcanic systems in Iceland = Upptok jardskjalfta 1982-1985 og eldstodvakerfi a Islandi [Map]. Menningarsjóður, 1987.
Einarsson, S.: Brennisteinsfjöll Alternative name: Bláfjöll, in: Catalogue of Icelandic volcanoes, edited by: Óladóttir, B. A., Larsen, G., and Gudmundsson, M. T., IMO, UI and CPD-NCIP, Retrieved from http://icelandicvolcanoes.is/?volcano=BRE#, 2019a.

Einarsson, S.: Krýsuvík-Trölladyngja Alternative name: Krísuvík, in: Catalogue of Icelandic volcanoes, edited by: Óladóttir, B. A., Larsen, G., and Gudmundsson, M. T., IMO, UI and CPD-NCIP, Retrieved from http://icelandicvolcanoes.is/?volcano=KRY#, 2019b.

Favalli, M., Pareschi, M. T., Neri, A., and Isola, I.: Forecasting lava flow paths by a stochastic approach. Geophysical Research Letters, 32(3). https://doi.org/10.1029/2004GL021718, 2005.

Favalli, M., Tarquini, S., Papale, P., Fornaciai, A., and Boschi, E.: Lava flow hazard and risk at Mt. Cameroon volcano, Bull Volcanol, 74, 423–439, https://doi.org/10.1007/s00445-011-0540-6, 2012.

Felpeto, A., Martí, J., and Ortiz, R.:Automatic GIS-based system for volcanic hazard assessment. Journal of Volcanology and Geothermal Research, 166, 106-116. Doi:10.1016/j.jvolgeores.2007.07.008, 2007.

Flóvenz, Ó. G., Wang, R., Hersir, G. P., Dahm, T., Hainzl, S., Vassileva, M., Drouin, V., Heimann, S., Isken, M. P., Gudnason, E. Á., Ágústsson, K., Ágústsdóttir, T., Horálek, J., Motagh, M., Walter, T. R., Rivalta, E., Jousset, P., Krawczyk, C. M., and Milkereit, C.: Cyclical geothermal unrest as a precursor to Iceland's 2021 Fagradalsfjall eruption. Nature Geoscience, 15(5), 397–404. https://doi.org/10.1038/s41561-022-00930-5, 2022.

Flynn, I. T., Chevrel, M. O., Crown, D. A., & Ramsey, M. S.: The effects of digital elevation model resolution on the PyFLOWGO thermorheological lava flow model. Environmental Modelling & Software, 105768. https://doi.org/10.1016/j.envsoft.2023.105768, 2023.

Ganci, G., Vicari, A., Cappello, A., & Del Negro, C.: An emergent strategy for volcano hazard assessment: From thermal satellite monitoring to lava flow modeling. Remote Sensing of Environment, 119, 197–207. https://doi.org/10.1016/j.rse.2011.12.021, 2012.

Gee, M. A. M.: Volcanology and geochemistry of Reykjanes Peninsula: Plume-mid-ocean ridge interaction. [PhD]. University of London, 1998.

Glaze, L. S., and Baloga, S. M.: Simulation of inflated pahoehoe lava flows. Journal of Volcanology and Geothermal Research, 255, 108–123. https://doi.org/10.1016/j.jvolgeores.2013.01.018, 2013.

Greenfield, T., Winder, T., Rawlinson, N., Maclennan, J., White, R. S., Ágústsdóttir, T., Bacon, C. A., Brandsdóttir, B., Eibl, E. P. S., Glastonbury-Southern, E., Gudnason, E. Á., Hersir, G. P., and Horálek, J.: Deep long period seismicity preceding and during the 2021 Fagradalsfjall eruption, Iceland, Bull Volcanol, 84, 101, https://doi.org/10.1007/s00445-022-01603-2, 2022.

Harris, A. J., and Rowland, S.: FLOWGO: A kinematic 23hermos-rheological model for lava flowing in a channel. Bulletin of Volcanology, 63(1), 20–44. https://doi.org/10.1007/s004450000120, 2001.

Harris, A. J. L., Villeneuve, N., Di Muro, A., Ferrazzini, V., Peltier, A., Coppola, D., Favalli, M., Bachèlery, P., Froger, J.-L., Gurioli, L., Moune, S., Vlastélic, I., Galle, B., and Arellano, S.: Effusive crises at Piton de la Fournaise 2014-2015: a review of a multi-national response model. Journal of Applied Volcanology, 6(1), 11. https://doi.org/10.1186/s13617-017-0062-9, 2017.

Harris, A.J.L., Chevrel, M. O., Coppola, D., Ramsey, M. S., Hrysiewicz, A., Thivet, S., Villeneuve, N., Favalli, M., Peltier, A., Kowalski, P., DiMuro, A., Froger, J.-L., and Gurioli, L.: Validation of an integrated satellite-data-driven response to an effusive crisis: the April–May 2018 eruption of Piton de la Fournaise. Annals of Geophysics, 61. https://doi.org/10.4401/ag-7972, 2019.

Jakobsson, S. P., Jónsson, J., and Shido, F.: Petrology of the Western Reykjanes Peninsula, Iceland. Journal of Petrology, 19(4), 669–705. https://doi.org/10.1093/petrology/19.4.669, 1978.

Jones, J. G.: Intraglacial volcanoes of the Laugarvatn region, south-west Iceland—I. Quarterly Journal of the Geological Society, 124(1–4), 197–211. https://doi.org/10.1144/gsjgs.124.1.0197, 1969.

Jónsson, J.: Jarðfræðikort af Reykjanesskaga (Geological map of the Reykjanes Peninsula). Orkustofnun Jarðhitadeilsd 7831, 1978.

Jóhannesson, T., Björnsson, H., Magnusson, E., Gudmundsson, S., Palsson, F., Sigurdsson, O., Throsteinsson, Th. And Berthier, E.: Ice-volume changes, bias estimation of mass-balance measurements and changes in subglacial lakes derived by lidar mapping of the surface of23hermos23nc glaciers. Annals of Glaciology, 54 (63), 63–74, 2013.

Kauahikaua, J.: Lava flow hazard assessment, as of August 2007, for Kilauea east rift zone eruptions, Hawaii island. U.S. Geological Survey Open-File Report 2007-1264, August, 9 p. http://www.usgs.gov/pubprod, 2007.

Klein, F. W., Einarsson, P., and Wyss, M.:The Reykjanes Peninsula, Iceland, earthquake swarm of September 1972 and its tectonic significance. Journal of Geophysical Research (1896-1977), 82(5), 865–888. https://doi.org/10.1029/JB082i005p00865, 1977.

Lowenstern, J. B., Wallace, K., Barsotti, S., Sandri, L., Stovall, W., Bernard, B., Privitera, E., Komorowski, J.-C., Fournier, N., Balagizi, C., and Garaebiti, E.: Guidelines for volcano-observatory operations during crises: recommendations from the 2019 volcano observatory best practices meeting, Journal of Applied Volcanology, 11, 3, https://doi.org/10.1186/s13617-021-00112-9, 2022

Martí, J., Becerril, L., and Rodríguez, A.: How long-term hazard assessment may help to anticipate volcanic eruptions: The case of La Palma eruption 2021 (Canary Islands), Journal of Volcanology and Geothermal Research, 431, 107669, https://doi.org/10.1016/j.jvolgeores.2022.107669, 2022.

Mossoux, S., Saey, M., Bartolini, S., Poppe, S., Canters, F., and Kervyn, M.: Q-LAVHA: A flexible GIS plugin to simulate lava flows. Computers & Geosciences, 97, 98–109. https://doi.org/10.1016/j.cageo.2016.09.003, 2016.

Neal, C. A., Brantley, S. R., Antolik, L., Babb, J. L., Burgess, M., Calles, K., Cappos, M., Chang, J. C., Conway, S., Desmither, L., Dotray, P., Elias, T., Fukunaga, P., Fuke, S., Johanson, I. A., Kamibayashi, K., Kauahikaua, J., Lee, R. L., Pekalib, S., … Damby, D.: The 2018 rift eruption and summit collapse of Kīlauea Volcano. Science, 363(6425), 367–374. https://doi.org/10.1126/science.aav7046, 2019.

Óladóttir, B. A., Óladóttir, B. A., Larsen, G., and Gudmundsson, M. T.: Fagradalsfjall Also known as part of Krýsuvík-Trölladyngja volcanic system, in: Catalogue of Icelandic volcanoes, IMO, UI and CPD-NCIP, Retrieved from http://icelandicvolcanoes.is/?volcano=FAG#, 2022.

Pallister, J., Papale, P., Eichelberger, J., Newhall, C., Mandeville, C., Nakada, S., Marzocchi, W., Loughlin, S., Jolly, G., Ewert, J., and Selva, J.: Volcano observatory best practices (VOBP) workshops—A summary of findings and best-practice recommendations. Journal of Applied Volcanology, 8(1), 2. https://doi.org/10.1186/s13617-019-0082-8, 2019.

Pedersen, G. B. M., and Grosse, P.: Morphometry of subaerial shield volcanoes and glaciovolcanoes from Reykjanes Peninsula, Iceland: Effects of eruption environment. Journal of Volcanology and Geothermal Research, 282, 115–133. https://doi.org/10.1016/j.jvolgeores.2014.06.008, 2014.

Pedersen, G. B. M., Belart, J. M. C. Óskarsson, B. V., Gudmundsson, M. T., Gies, N., Högnadóttir, Th., Hjartardóttir, A. R., Pinel, V., Berthier, E., Dürig, T., Reynolds, H. I., Hamilton, C. W., Valsson, G., Einarsson, P., Ben-Yehosua, D., Gunnarsson, D., Oddsson, B.: Volume, effusion rate, and lava transport during the 2021 Fagradalsfjall eruption: Results from near real-time photogrammetric monitoring. Geophisical Research Letters, doi:10.1029/2021GL097125, 2022a.

Pedersen, G. B. M., Belart, J. M.C., Óskarsson, B. V., Gudmundsson, M. T., Gies, N., Högnadóttir, Th., Hjartadótti, Á. R. Pinel, V., Berthier, E., Dürig, T., Reynolds, H. I., Hamilton, C. W., Valsson, G., Einarsson, P., Ben-Yehosua, D., Gunnarsson, A., and Oddsson, B.: Digital Elevation Models, orthoimages and lava outlines of the 2021 Fagradalsfjall eruption: Results from near real-time photogrammetric monitoring (Version v1) [Data set]. Zenodo. https://doi.org/10.5281/zenodo.6581470, 2022b.

Peltier, A., Ferrazzini, V., Di Muro, A., Kowalski, P., Villeneuve, N., Richter, N., Chevrel, M. O., Froger, J.-L., and Hrysiewicz A, Gouhier M, Coppola D, Retailleau L, Beauducel F, Boissier P, Brunet C, Catherine P, Fontaine F, Lauret F, Garavaglia L, Lebreton J, Canjamale K, Desfete N, Griot C, Arellano S and Liuzzo M, G. S.: Volcano crisis management during COVID-19 lockdown at Piton de la Fournaise (La Réunion). Seismological Research Letters, On line No, 1–15. https://doi.org/10.1785/0220200212, 2020.

Peltier, A, Chevrel, M. O., Harris, A. J. L., and Villeneuve, N.: Reappraisal of gap analysis for effusive crises at Piton de la Fournaise. Journal of Applied Volcanology, 11(1), 1–17. https://doi.org/10.1186/s13617-021-00111-w, 2022.

Pfeffer, M. A., Barsotti, S., Karlsdóttir, S., Jensen, E. H., Pagneux, E. P., Björnsson, B. B., Jóhannesdóttir, G., Höskuldsson, Á., Sandri, L., Selva, J., and Tarquini, S.: An initial volcanic hazard assessment of the Vestmannaeyjar Volcanic System. Icelandic Meterological Office, Iceland, 73 pp., 2020.

~~Pierrot-Deseilligny, M., and Clery, I.: Apero, an open source bundle adjustment software for automatic calibration and orientation of set of images. Int. Arch. Photogr. Remote Sens. Spat. Inform. Sci. 3816, 269–276. Doi: 10.5194/isprsarchives-XXXVIII-5-W16-269-2011, 2011.~~

Porter, C., Morin, P., Howat, I., Noh, M.-J., Bates, B., Peterman, K., et al.: ArcticDEM. Harvard Dataverse, V1. Polar Geospatial Center, University of Minnesota. Doi: 10.7910/DVN/OHHUKH, 2018.

Richter, N., Favalli, M., de Zeeuw-van Dalfsen, E., Fornaciai, A., da Silva Fernandes, R. M., Pérez, N. M., Levy, J., Victória, S. S., and Walter, T. R.: Lava flow hazard at Fogo Volcano, Cabo Verde, before and after the 2014–2015 eruption, Natural Hazards and Earth System Sciences, 16, 1925–1951, https://doi.org/10.5194/nhess-16-1925-2016, 2016.

Rossi, M. J.: Morphology and mechanism of eruption of postglacial shield volcanoes in Iceland. Bulletin of Volcanology, 57(7), 530–540. https://doi.org/10.1007/BF00304437, 1996.

~~Rupnik, E., Daakir, M., and Pierrot Deseilligny, M.: MicMac – a free, open-source solution for photogrammetry. Open Geospatial Data Softw. Stand. 2:14. Doi: 10.1186/s40965-017-0027-2, 2017.~~

Sigmundsson, F., Parks, M., Hooper, A., Geirsson, H., Vogfjörd, K. S., Drouin, V., Ófeigsson, B. G., Hreinsdóttir, S., Hjaltadóttir, S., Jónsdóttir, K., Einarsson, P., Barsotti, S., Horálek, J., and Ágústsdóttir, T.: Deformation and seismicity decline before the 2021 Fagradalsfjall eruption, Nature, 609, 523–528, https://doi.org/10.1038/s41586-022-05083-4, 2022.

Sigurgeirsson, M. A. and Einarsson, S.: Reykjanes and Svartsengi volcanic systems. In: Oladottir, B., Larsen, G. and Guðmundsson, M. T.: Catalogue of Icelandic Volcanoes. IMO, UI and CPD-NCIP. Retrieved from http://icelandicvolcanoes.is/?volcano=REY#, 2016.

Sæmundsson, K.: Hengill, in: Catalogue of Icelandic volcanoes, edited by: Óladóttir, B. A., Larsen, G., and Gudmundsson, M. T., IMO, UI and CPD-NCIP, Retrieved from http://icelandicvolcanoes.is/?volcano=HEN#, 2019.

Sæmundsson, K., Jóhanneson, H., Hjartarson, Á., Kristinsson, S. G., & Sigurgeirsson, M. Á.: Geologic map of Southwest Iceland. [Map]. Iceland Geosurvey, 2010.

Sæmundsson, K. and Sigurgeirsson, M. Á.: Reykjanesskagi, in: Náttúruvá, edited by: Sólnes, J., Sigmundsson, F., and Bessason, B., Viðlagatrygging Íslands / Háskólaútgáfa, 379–401, 2013.

Sæmundsson, K., Sigurgeirsson, M. Á., and Friðleifsson, G. Ó.: Geology and structure of the Reykjanes volcanic system, Iceland. Journal of Volcanology and Geothermal Research, 391, 106501, 2020. https://doi.org/10.1016/j.jvolgeores.2018.11.022, 2020.

Tarquini, S., and Favalli, M.: Uncertainties in lava flow hazard maps derived from numerical simulations: The case study of Mount Etna. Journal of Volcanology and Geothermal Research, 260, 90–102. https://doi.org/10.1016/j.jvolgeores.2013.04.017, 2013.

Tarquini, S., Vitturi, M. de' M., Jensen, E., Pedersen, G., Barsotti, S., Coppola, D., and Pfeffer, M. A.: Modeling lava flow propagation over a flat landscape by using MrLavaLoba: The case of the 2014–2015 eruption at Holuhraun, Iceland. Annals of Geophysics, 62(2), VO228–VO228. https://doi.org/10.4401/ag-7812, 2019.

Thorkelsson, B. (ed.): The 2010 Eyjafjallajökull eruption, Iceland. Report to ICAO – June 2012. Icelandic Meteorological Office, University of Iceland. Institute of Earth Sciences, The National Commissioner of the Icelandic Police, Reykjavík. IVATF 4-IP/3, 206 s. Steering and editorial committee: Sigrún Karlsdóttir (chair), Ágúst Gunnar Gylfason, Ármann Höskuldsson, Bryndís Brandsdóttir, Evgenia Ilyinskaya, Magnús Tumi Guðmundsson and Þórdís Högnadóttir, 2012.

Vicari, A., Ganci, G., Behncke, B., Cappello, A., Neri, M., and Del Negro, C.: Near-real-time forecasting of lava flow hazards during the 12–13 January 2011 Etna eruption. Geophysical Research Letters, 38(13). https://doi.org/10.1029/2011GL047545, 2011.

Wright, R., Garbeil, H., and Harris, A. J. L.: Using infrared satellite data to drive a 25hermos-rheological/stochastic lava flow emplacement model: A method for near-real-time volcanic hazard assessment. Geophysical Research Letters, 35(19), 1–5. https://doi.org/10.1029/2008GL035228, 2008.

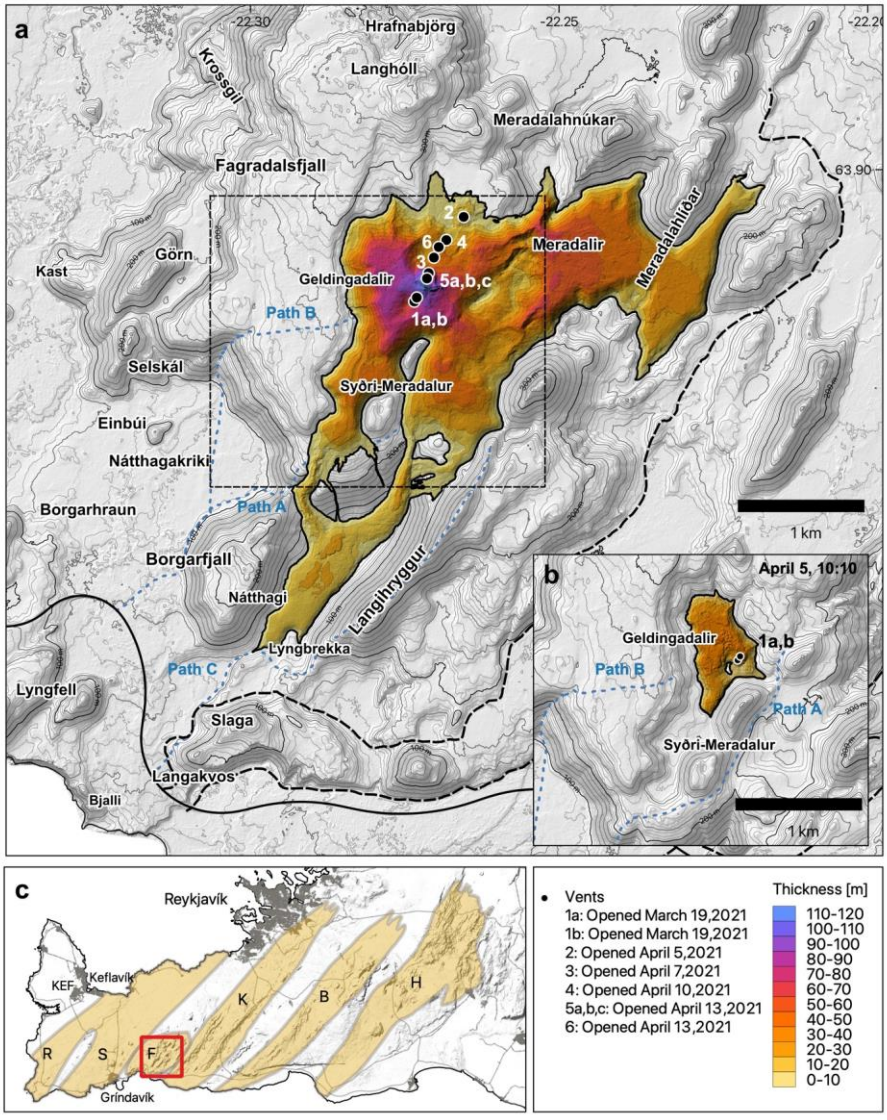
a
-22.30
-22.25
Hrafnabjörg
Krossgil
Langhóll
Meradalahnúkar
Fagradalsfjall
63.90
2
6
4
3
5a,b,c
1a,b
Meradalir
Meradalahlíðar
Geldingadalir
Path B
Kast
Görn
Selskál
Einbúi
Nátthagakriki
Syðri-Meradalur
Borgarhraun
Path A
1 km
Borgarfjall
Nátthagi
Langihryggur
Lyngbrekka
Path C
Lyngfell
Slaga
Langakvos
Bjalli
b
April 5, 10:10
Geldingadalir
1a,b
Path B
Path A
Syðri-Meradalur
1 km
c
Reykjavík
KEF
Keflavík
K
B
H
R
S
F
Grindavík
Vents
1a: Opened March 19,2021
1b: Opened March 19,2021
2: Opened April 5,2021
3: Opened April 7,2021
4: Opened April 10,2021
5a,b,c: Opened April 13,2021
6: Opened April 13,2021
Thickness [m]
110-120
100-110
90-100
80-90
70-80
60-70
50-60
40-50
30-40
20-30
10-20
0-10

Figure 1: a) Overview of the Fagradalsfjall area at the end of the eruption. Vents are marked with dots and numbered chronologically after opening time. The lava thickness map is from September 30, 2021 (Pedersen et al., 2022b). Dashed black box indicates the extent of frame b. The highway is marked with a solid black line, and dirt roads with dashed black lines. ~~Hiking paths~~ are shown in dashed blue. b) Overview of the Fagradalsfjall area by the end of Phase 1. The lava thickness map is from April 5, 2021 (Pedersen et al., 2022b). ~~Hiking paths are shown in dashed blue.~~ C) Map of the Reykjanes Peninsula. The red box indicates the area displayed in a). Densely populated areas are marked in gray. Volcanic systems (Sæmundsson and Sigurgeirsson, 2013, fig. 4.13.1) are marked orange and denoted by capital letters according to their name; R: Reykjanes, S: Svartsengi, F: Fagradalsfjall, K: Krýsuvík, B: Brennisteinsfjöll, H: Hengill. Background topography is based on the IslandsDEM (Porter et al., 2018).

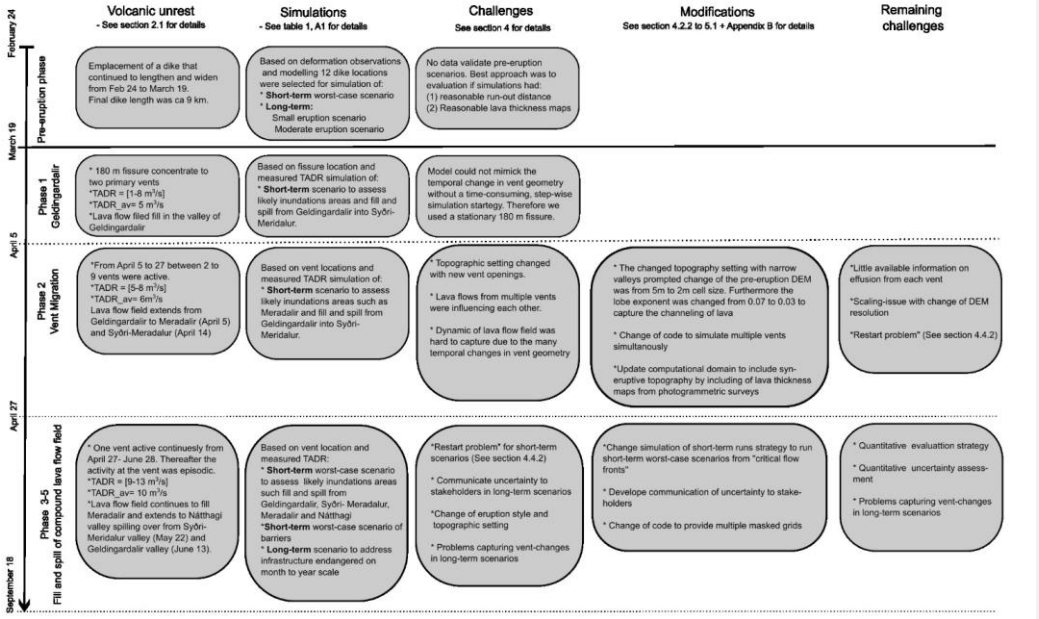

Figure 2: Illustration of the temporal development of the volcanic unrest (first column), the simulations performed addressing these developments (column 2), the identified simulation challenges (column 3), the modifications implemented to address these challenges (column 4) and the remaining challenges.

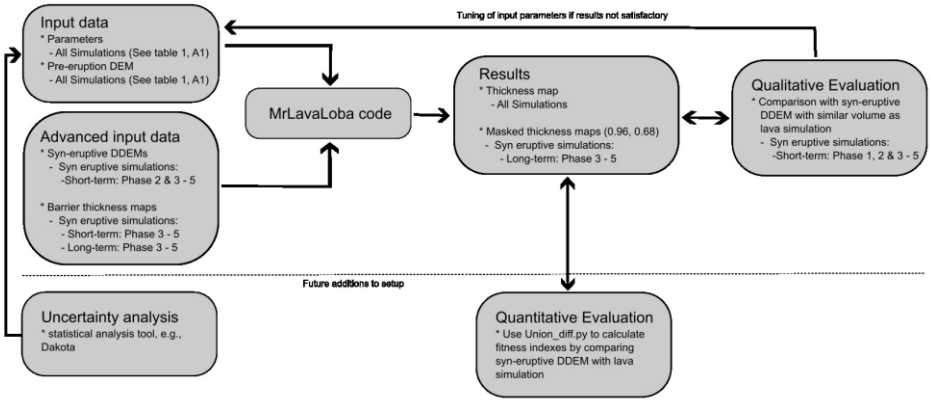

Figure 3: Flow chart for the lava flow simulations performed with the MrLavaLoba code during the Fagradalsfjall 2021 volcanic unrest. Suggested future improvements of the setup is added below the dashed line.

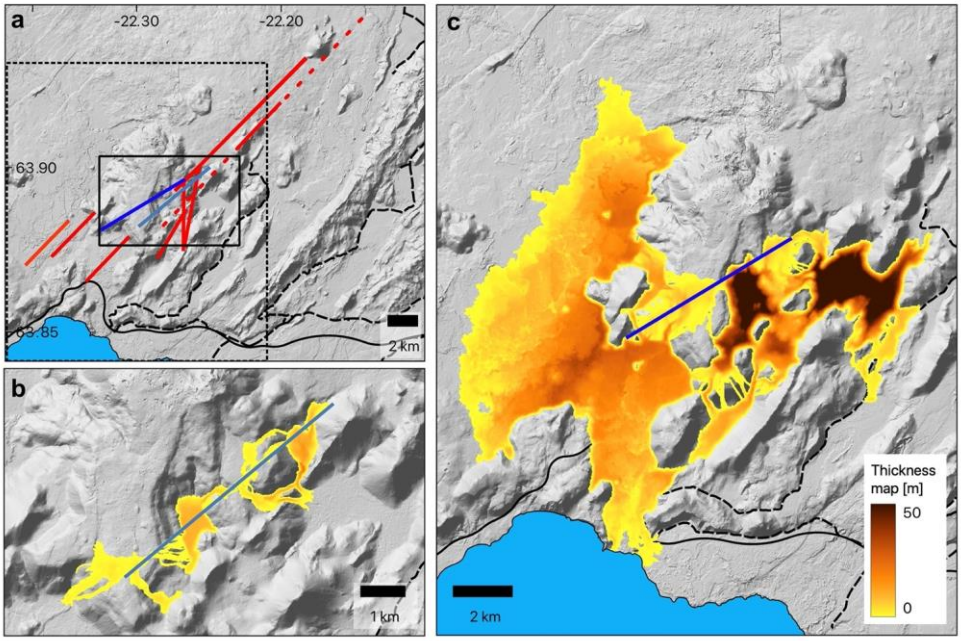

Figure 4: (a) Overview of modeled pre-eruption potential fissures (red, light blue for fissure in frame b and dark blue for fissure in frame c). Solid black box indicates the extent of frame b and dashed black box indicates the extent of frame c. The highway is marked with a solid black line, and dirt roads with dashed black lines. (b) ~~Worst-case~~Short-term large effusion rate scenario (300 m^3/s) for t= 180 min for a pre-eruption fissure (light blue). (c) Moderate scenario (0.3 km^3) run for a pre-eruption fissure (dark blue). Background topography is based on the IslandsDEM (Porter et al., 2018).

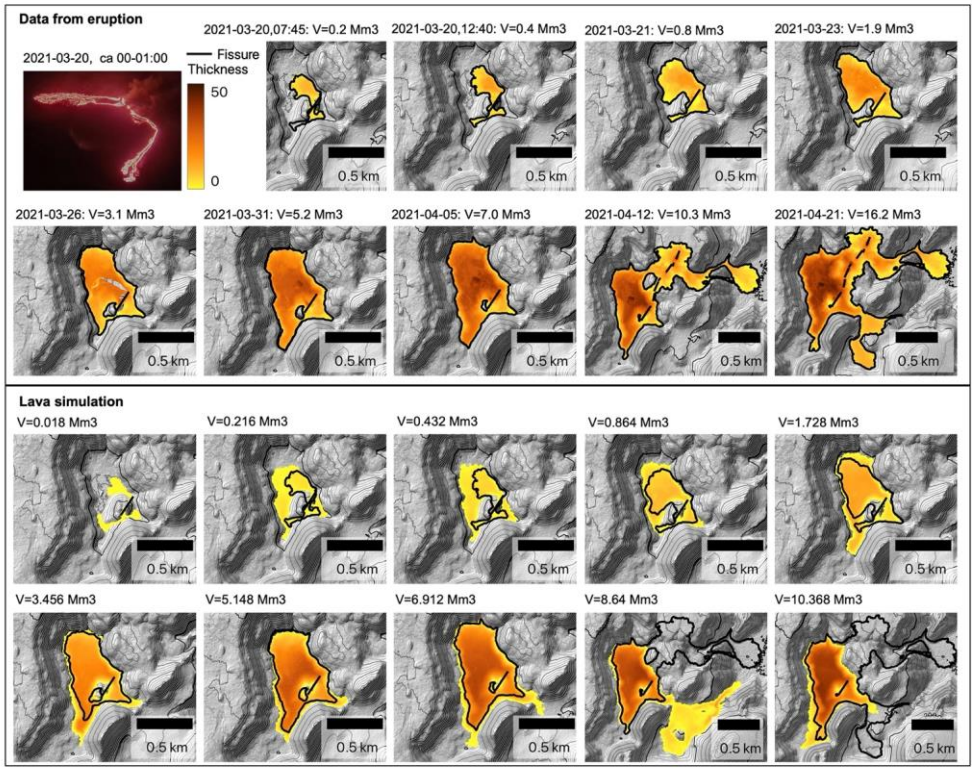

Figure 5: Comparison between thickness maps obtained from the lava field (Upper box) in the first 24 days of the eruption (Pedersen et al., 2022b) and lava simulation thickness maps (Lower box). The volume of each thickness map is noted above each map. Thickness scale is the same for DDEMs and lava simulation thickness maps. The initial length of the first fissure is marked as a black line. The last two frames showing thickness maps from the eruption extend into phase 2 and therefore also include the fissures that opened in phase 2. Background topography is based on the IslandsDEM (Porter et al., 2018). Photo in the top left is by Freysteinn Sigmundsson.

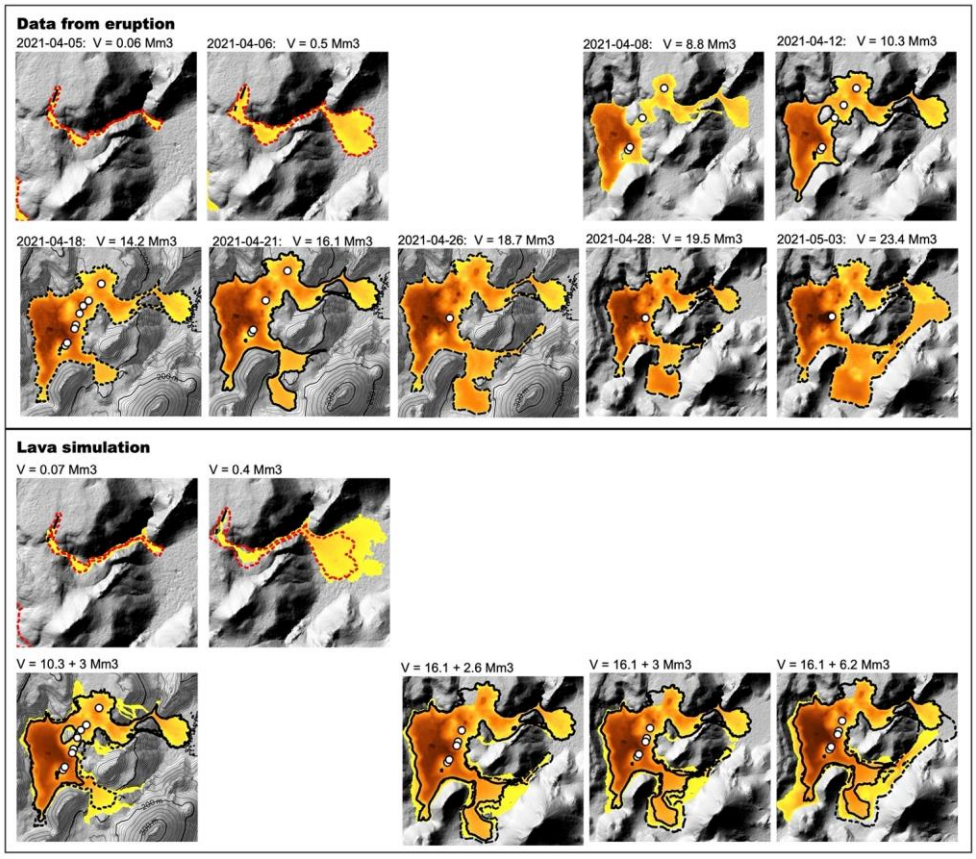

Figure 6: Comparison between thickness maps obtained from the lava field (Pedersen et al., 2022b) from April 5 to May 3 (Upper box) and lava simulation thickness maps performed during the vent migration phase (Lower box). The lava simulations in the bottom panel show the cumulative thickness of the syn-eruptive thickness map and the results from the simulation. The volume of each thickness map is noted above each map, which for the cumulative thickness maps is split into the volume contribution from the syn-eruptive thickness map and the simulation (e.g., V=16.1 + 6.2 Mm^3). The thickness scale is the same for DDEMs and lava simulation thickness maps going from 0 m (yellow) to 50 m (brown). The extent of the thickness maps used as input to the simulation has a solid black outline, while the extent of the lava thickness maps from the lava field with comparable volume is marked with hatched outlines. The active vents are in white, except for fissure 2 (top left), where the initial two fissure segments are shown as black lines. Background topography is based on the IslandsDEM (Porter et al., 2018).

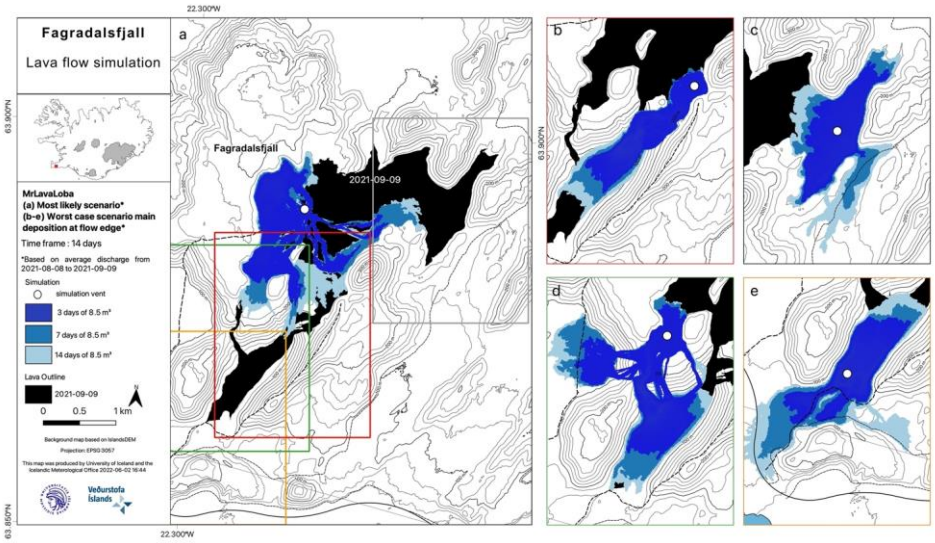

Figure 7: An example of how the short-term worst-case scenarios were presented. Example from 9 September, 2021. (a) Simulation from vent 5, which was considered the most likely scenario. (b) Worst-case scenario for Syðri-Meradalur to investigate if lava could exit the valley through the saddle point to the southeast. Based on these results the lava seemed more likely to exit south to Nátthagi. (c) Worst-case scenario for Meradalir to investigate if lava would spill to the east out of the valleys. Based on the results this was considered an option given most of the erupted volume would reach Meradalir. (d) Worst-case scenario for Geldingadalir to investigate if lava would spill to the southwest into Nátthagakriki over the build barriers. Based on the results this was considered an option. (e) Worst-case scenario for Nátthagi to investigate if lava would spill to the south out of the valley. Based on the results this was considered an option given most of the erupted volume would reach Nátthagi. Background topography is based on the IslandsDEM (Porter et al., 2018).

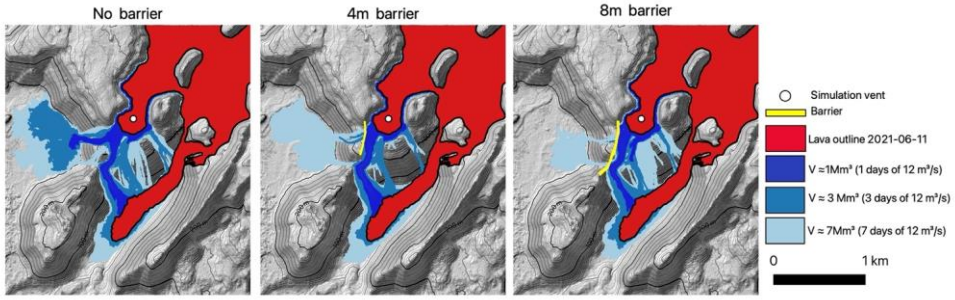

Figure 8: An example of lava simulations predicting how Geldingadalir would overflow with and without lava barriers. The simulation vent is located in southern Geldingadalir based on observation of lava inflation in that area. Data based on survey from June 11, 2021 and the calculated volumes and time scales are based on the estimated TADR from the same survey. Background topography is based on the IslandsDEM (Porter et al., 2018).

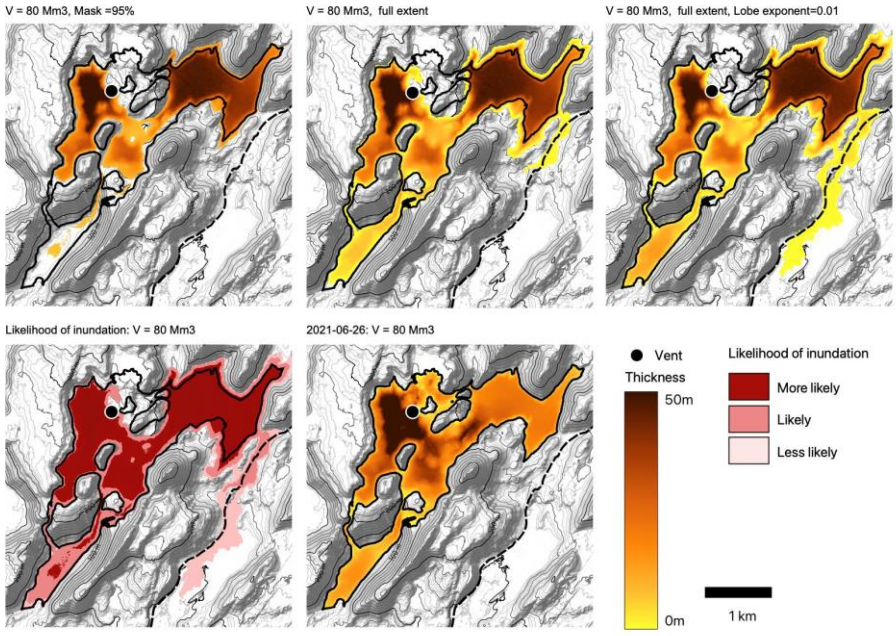

Figure 9: Top row: Example of the best tuning result for the 80 Mm3 simulation showing the 95 % lava thickness mask representing the category "More likely" and the full extent representing "Likely" category. To the right is a 80 Mm^3 simulation result with a lower lobe exponent representing the "Less likely" category. Bottom row: Map showing the likelihood of inundation based on the 80 Mm^3 simulations shown in the top row (Left) and lava thickness map from 2021-06-26 (Pedersen et al., 2022b), which can be compared to the simulation results in the top row (Right). Background topography is based on the IslandsDEM (Porter et al., 2018).

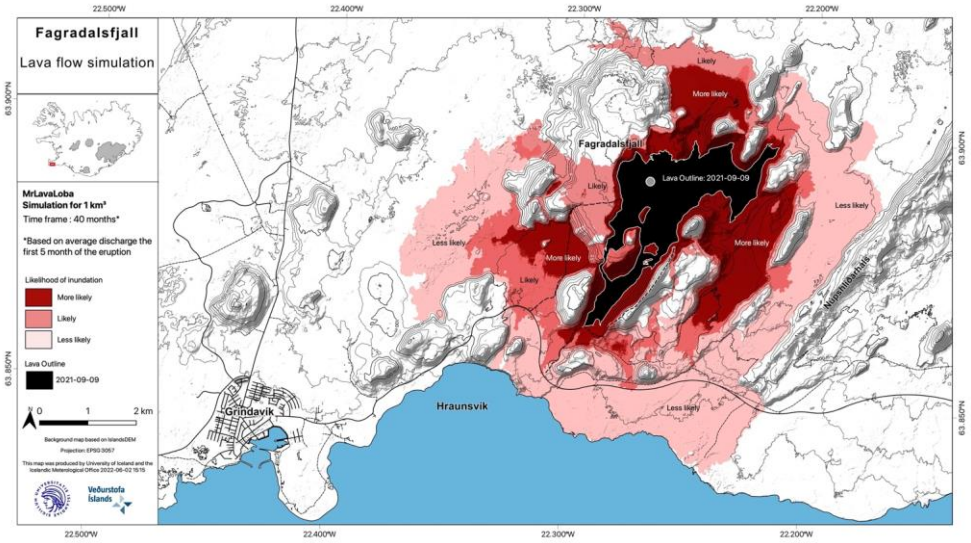

915

Figure 10: Long-term scenario for lava emplacement of 1000 Mm^3 volume issued from vent 5. Background topography is based on the IslandsDEM (Porter et al., 2018).

Table 1 Overview of implementation strategies of MrLavaLoba for pre- and syn-eruptive simulations

	Pre-eruptive simulations			**Syn-eruptive simulations**			
	Short -term	**Longer-term**		**Short -term**			**Longer-term**
	Worst-case scenario	Small eruption scenario	Moderate eruption scenario	Phase 1: Geldingadalir	Phase 2: Vent migration	Phase 3-5: Compound lava field	Phase 3-5: Compound lava field
Goal	Assess likely areas inundated hours after eruption start of high-effusion rate eruption	Gain insight to areas likely to be inundated within weeks from eruption start	Gain insight to areas likely to be inundated months after eruption start	Assess likely areas inundated first weeks of the eruption, including when Geldingadalir would spill into Syðri-Meradalur	Assess likely areas inundated during vent migration period, including when Geldingadalir would spill into Syðri-Meradalur	Forecast spilling of one valley to another. Evaluate areas endangered to lava inundation, specifically areas close to hiking paths/safety zones. Evaluate when barriers may be compromised	Address infrastructure endangered to lava flow inundation on month to year scale
Approach	Multiple runs with various volumes simulating V= Q x t, where Q= 300 m^3/s. Some of the input variables are made time-dependent	One run based on a pre-defined parameter space derived from scenarios compared with historical lava flows	One run based on a pre-defined parameter space derived from scenarios compared with historical lava flows	Multiple runs with various volumes simulating V= Q x t, where Q= TADR measurements from photogrammetric surveys. Some of the input variables are made time dependent.	Multiple runs with various volumes simulating V= Q x t, where Q= TADR measurements from photogrammetric surveys. Some of the input variables are made time dependent.	Multiple runs with various volumes simulating V= Q x t, where Q= TADR measurements from photogrammetric surveys. Some of the input variables are made time-dependent	Multiple runs with various volumes () simulating V= Q*t, where Q= TADR_mean for the eruption. All input parameters were tuned based on lava thickness maps obtained in June having volumes between 53-80 Mm^3
Evaluation	Lava run out length + lava thickness	Tuning compared to Illahraun (historical scenario)	Tuning compared to Arnaseturhraun (historical scenario)	Qualitative comparison to lava thickness maps	Qualitative comparison to lava thickness maps	NA	The eruption stopped at V= 150 Mm^3 and thus not comparable to our smallest long-term scenarios (250Mm^3)
DEM	Pre-eruption DEM (5 m x 5 m)	Pre-eruption DEM (10 m x 10 m)	Pre-eruption DEM (10 m x 10 m)	Pre-eruption DEM (5 m x 5 m)	Pre-eruption DEM (2 m x 2 m) / Pre-eruption DEM (5 m x 5 m) + DDEM from 2021-04-12 (5 m x 5 m) / Pre-eruption DEM (5 m x 5 m) + DDEM from 2021-04-21 (5 m x 5 m)	Pre-eruption DEM + newest thickness map + thickness map of lava barriers (if relevant)	Pre-eruption DEM (10 m x 10 m) + newest thickness map + thickness map of lava barriers (if relevant)
Description of ~~Vents~~vents	2 km or ~~/~~ 10 km fissures (See Fig. 4a)	2 km or ~~/~~ 10 km fissures~~-~~ ~~—~~(See Fig. 4a)	2 km or ~~/~~ 10 km fissures ~~—~~(See Fig. 4a)	180 m fissure	Fissure 2 or ~~/~~All vents or~~/~~ 5 southernmost vents	Vent 5 or ~~/ Critical~~ critical lava margins	Vent 5
Variable Parameters							
t [min]	30, 60, 180 (360, 720)	NA	NA	t= V/ 10m3/s	t= V/ 5m3/s / t= V/ 8m3/s / t= V/ 5.1m3/s	3, 7, 14 days. Potentially 6 hr, 12 hr	t= V/ TADR_mean

						and 24 hr scenarios if needed.	
Volume [m3]	300 m^3/s * t*60s	0.02	0.3	0 - 10 Mm^3	0 - 2.6 Mm^3 /0 - 3 Mm^3/ 0 - 6 Mm^3/	TADR m^3/s * t*60s	150 Mm^3, 250 Mm^3, 350Mm^3, 500 Mm^3, 1000Mm^3, 5000 Mm^3
n flows	150 per km fissure	400	1600	10	10 / 80/80	160	2000 / (3000 for >1000 Mm^3)
minimum n lobes	3.33 x t	400	1500	2 x t[min]	2 x t[min] / 2 x t[min] / 1 x t[min]	1 x t [min]	3500
Lobe exponent	0.07	0.03	0.015	0.07	0.03/ 0.07/ 0.07	0.05	0.02 / 0.01

920

Table 2: Overview of advantages and disadvantages of the MrLavaLoba code

MrLavaLoba code	
Advantages	**Disadvantages**
• Free and easy to run in python • Very flexible and can be used for various simulation purposes • Fast computational time • Can run very large scenarios • Change topography during model run • Produce lava thickness layer • Includes volume + final extent • Can be used to assess infilling of depressions, valleys and overflows of barriers • Can handle multiple vents • Easy to implement barriers & new topography/thickness layer	• Input parameters have to be tuned to: known scenarios, individual eruptions, specific to type of activity and different topographic setting • Do not provide time/velocity evolution of lava emplacement in a single run • Do only mimic channel/tube formation if tuned for that,- does not develop inherently in the model • Do not include vent processes→ underestimate thickness of deposits close to the vent (thus DDEM should be implemented to account for that) • Results not designed for hazard communication and templates to develop simple maps for hazard communication had to be produced.

Appendix A

Table A1: Overview of all input parameters used depending on modelling approach. M: 1000000, t: time

Tuning Parameters	**Pre-eruptive simulations**			**Syn-eruptive simulations**			
	Short -term	**Longer-term**		**Short -term**			**Longer-term**
	Worst-case scenario: 300 m3/s	Small eruption scenario	Moderate eruption scenario	Phase 1: Geldingardalir	Phase 2:Vent migration	Phase 3-5: Compound lava field	Phase 3-5: Compound lava field
source DEM [in EPSG 3057]	Pre-eruption DEM (5 m x 5 m)	Pre-eruption DEM (10 m x 10 m)	Pre-eruption DEM (10 m x 10 m)	Pre-eruption DEM (5 m x 5 m)	Pre-eruption DEM (2 m x 2 m)/ Pre-eruption DEM (5 m x 5 m) + DDEM from 2021-04-12 (5 m x 5 m) / Pre-eruption DEM (5 m x 5 m) + DDEM from 2021-04-21 (5 m x 5 m)	Pre-eruption DEM + newest thickness map + thickness map of lava barriers (if relevant)	Pre-eruption DEM (10 m x 10 m) + newest thickness map + thickness map of lava barriers (if relevant)
vent_flag	2	2	2	2	7	7	7
x_vent [in EPSG 3057]	[x1, x2] 2/ 10 km fissures (See Fig. 4a)	[x1, x2] 2/ 10 km fissures (See Fig. 4a)	[x1, x2] 2/ 10 km fissures (See Fig. 4a)	[339326 ,339423]	Combination of following vents: [339366, 339386, 339522, 339489, 339467, 339473, 339545]	[339048]	[339048]
y_vent [in EPSG 3057]	[y1, y2] 2/ 10 km fissures (See Fig. 4a)	[y1, y2] 2/ 10 km fissures (See Fig. 4a)	[y1, y2] 2/ 10 km fissures (See Fig. 4a)	[380202 ,380364]	Combination of following vents: [380288, 380319, 380637, 380515, 380471, 380440, 380695]	[380058]	[380058]
hazard_flag	1	1	1	1	1	1	1
fissure_probabilities	NA	NA	NA	NA	[1, 1, 1, 5, 5, 5, 1]	[1]	[1]
masking_threshold	0.96	0.96	0.96	0.96	0.96	[0.68 ,0.96]	0.95
n_flows	150 per km fissure	400	1600	10	10 / 80/80	160	1000
min_n_lobes	3.33 x t[min]	400	1500	2 x t[min]	2 x t[min] / 2 x t[min] / 1 x t[min]	1 x t [min]	3500
max_n_lobes	min_n_lobes	min_n_lobes	min_n_lobes	min_n_lobes	min_n_lobes	min_n_lobes	min_n_lobes
volume_flag	1	1	1	1	1	1	1
total_volume	300 m^3/s x t[s]	20M	300M	TADR [m^3/s] x t[s]	TADR [m^3/s] x t[s]	TADR [m^3/s] x t[s]	150 M, 250 M, 350M, 500 M, 1000M, 5000M
fixed_dimension_flag	1	1	1	1	1	1	1
lobe_area	250	1000	1000	250	250	250	1000
thickness_ratio	0.9	2	2	0.9	0.9	0.9	2
topo_mod_flag	2	2	2	2	2	2	2
n_flows_counter	1	1	1	1	1	1	1

n_lobes_counter	1	1	1	1	1	1	1
thickening_parameter	0.06	0.06	0.06	0.06	0.06	0.06	0.02
lobe_exponent	0.07	0.03	0.015	0.07	0.07	0.05	0.02
max_slope_prob	0.8	0.8	0.8	0.8	0.8	0.8	0.8
inertial_exponent	0.1	0.1	0.1	0.1	0.1	0.1	0.1

Appendix B

In this appendix we describe the modifications implemented in the code MrLavaLoba to improve its usage during and after the 2021 Fagradalsfjall eruption. These changes have been uploaded to the MrLavaLoba Github repository (https://github.com/demichie/MrLavaLoba) as commits, which are records with unique ID, that identifies specific changes in github documents, when the changes were made and who made them. The code that has been added is highlighted in green, while code that has been deleted is in red.

1) April 2021 (commit 9f60549): Simulation of the whole ongoing eruption as a series of "phases".
This commit improved the usage of restart files, i.e., the possibility to start a new simulation including the output of a previous simulation. After this change the code allows to implement the simulation of the eruption as a series of "phases" without losing the benefit of the thickening parameter.

2) April 2021 (commits 80d4230, e2885d1, 9e1826c,23f6a16, 2311a50): Possibility to have multiple vents/fissures.

These commits enabled implementation of the possibility to consider multiple fissures/vents and to assign different probability to be active to each fissure. Here there is a list of the new conditions available:

- vent_flag = 4 => the initial lobes are on multiple fissures and all points of the fissures have the same probability that a “lobe chain” will start from them
- vent_flag = 5 => the initial lobes are on multiple fissures and all the fissures have the same probability that a “lobe chain” will start from them
- vent_flag = 7 => the initial lobes are on multiple fissures and the probability of each fissure is fixed by "fissure_probabilities"

3) September 2021 (commit 3c4e5d3): Enable multiple threshold values.

In addition to the final lava thickness map, the MrLavaLoba code allows saving masked grids obtained by considering inundated cells fulfilling a specified threshold value (de’ Michieli Vitturi and Tarquini, 2017). This is controlled by the input parameter masking_threshold, expressed in fraction of the total volume (i.e., varying within the interval [0; 1]). As an example, if the cut is applied to the thickness and masking_threshold is set to 0.95, the thinnest portion of the final lava deposit representing 5% of the total volume emplaced is cut out from the results. In the original version of MrLavaLoba it was possible to set a single value of masking_threshold for each simulation, but with this commit it is possible to set multiple values and thus save multiple output raster files.

4) January 2022 (commits d6d0953, 08afee3): code optimization.

With these commits input parameters to crop the DEM file, and then the computational domain, have been introduced. This crop reduces the computational time when the DEM is large and the area covered by the flow is a lot smaller.
In addition, an analysis with a profiler identified the numpy function “copy”, used to create a copy of a Numpy array, which was a bottleneck of the code. For this reason, the code has been rewritten to reduce the call to this function. The two changes increased the speed of the code by a factor of 5 to 10. The optimization also allowed us to remove some input parameters that became unnecessary after the changes.